CHAPTER 7:

INFLUENCE OF FILL DEPTH AND FRICTION ANGLE

7.1 Introduction

This chapter describes an investigation into the plane strain response of the two-layer soil system for variations in both fill depth and fill strength. Through careful selection of these important design parameters, the maximum benefit can be obtained from including reinforcement within a two-layer soil system.

The typical reinforced two-layer soil system, described as the 'central parametric analysis' in Chapter 6, is used as the datum for this investigation with the material properties given in Appendix 6A. Three separate fill depths and friction angles are used in this study for both the reinforced and unreinforced cases. Table 7.1 gives the varying values of the fill depth D_f (m) and the plane strain fill friction angle ϕ_{PS} (degs) for the eighteen large strain finite element runs, (postscript 'R' designates reinforced). The different fill depths selected are representative of those thicknesses commonly used in practical and experimental unpaved roads and reinforced subsoil trials, as discussed in Chapter 2.

The friction angles used in this study cover the typical range of fill strengths that are encountered in two-layer soil systems. Milligan *et al.* (1989) proposes that, for an unpaved road, a fill strength of $\phi = 30°$ is "weak", $\phi = 38°$ is "normal" and $\phi = 45°$ is "strong". Poran (1985) suggests that the range of friction angles of dense granular materials are normally between 35° to 50° and he uses a triaxial friction angle of $\phi = 46°$ in the finite element model. Hird and Kwok (1990) use $\phi_{PS} = 40°$ in their embankment analysis, and Alenowicz and

Friction Angle ϕ_{PS}	Fill Depth D_f $0.6B = 0.15\,m$	$1.2B = 0.3\,m$	$2.0B = 0.5\,m$
30 °	A30 A30R	B30 B30R	C30 C30R
40 °	A40 A40R	B40 B40R	C40 C40R
55 °	A55 A55R	B55 B55R	C55 C55R

Table 7.1: Finite Element Run References

Dembicki (1990) use sand of $\phi = 30°$ in their experimental model temporary road tests. Furthermore, as stated in Chapter 6, Type 1 Subbase Material is typically used in unpaved roads (Specification for Highway Works (1986)), which has an average peak friction angle of between $\phi_{peak} = 46°$ and 56 °.

7.2 Fill Friction Angle

There is a variety of different instruments and methods available to measure the friction angle of a granular material and because ϕ is sensitive to these different methods a variety of different friction angle values can be obtained for one particular material. To avoid confusion the specific classification test method used must be stated in conjunction with the actual parameter of friction angle. For the particular finite element calculations undertaken in this study the triaxial compression friction angle, ϕ_T, is the required input parameter for the Matsuoka constitutive model used in OXFEM (see Chapter 3), and a conversion is then made so that the numerical calculations are actually for a specified plane strain friction angle.

The relationship between the triaxial and plane strain plasticity parameters of granular materials (i.e. ϕ_T, γ_a and ϕ_{PS}, ψ_{PS} respectively) is comprehensively discussed by Burd (1986), where a table of comparisons of ϕ_T and ϕ_{PS} is given for different values of dilation rate. The difference between triaxial and plane strain friction angles was also discussed by Wroth (1984), who proposed the linear empirical relationship:-

$$8\,\phi_{PS} \approx 9\,\phi_T \tag{7.1}$$

The dilation characteristics of the fill material are thought to have only a small influence on the load capacity behaviour of a soil under a footing, because the soil is relatively unrestrained kinematically compared to, say, the highly constrained soil near a pile (Houlsby (1991)). Therefore, the degree-of-association parameter (γ_a) is taken to be a constant value of 0.6 throughout this parametric study. An exhaustive review of how the dilatancy of soils effects their behaviour is made by Houlsby (1991).

7.3 Parametric Study

The following sections consider the effects of variations in both the fill depth and fill strength on the load-displacement response of the two-layer soil structure, the arrangement of stresses and displacements at the reinforced and unreinforced fill-clay interface and the reinforcement tension, as predicted by the finite element analysis. For comparison, the analytical results given by the Houlsby *et al.* (1989) method are also presented for the same variations in fill depth and strength. The effect on the load spread through the fill is also investigated, with comparisons made to previous experimental work and theoretical analyses.

7.3.1 Load-Displacement and Load Spread Responses

The load-displacement responses for each of the eighteen finite element runs listed in Table 7.1 are shown in Figure 7.1, where P is the vertical footing pressure and δ is the vertical footing displacement.

The final footing pressures, P_f, at a footing displacement of $\delta = 0.6\ B$ are listed in Table 7.2, along with the estimated load spread angles, β, (calculated as the 95% normal stress limit) and the angles of friction of the footing base, δ_f, (determined by the method discussed in Section 6.5.7) for each analysis. Additionally, the ultimate footing loads and the reinforcement forces predicted by the Houlsby *et al.* (1989) analytical method are also given in Table 7.2, calculated using the relevant angles of β, δ_f and ϕ_{PS}.

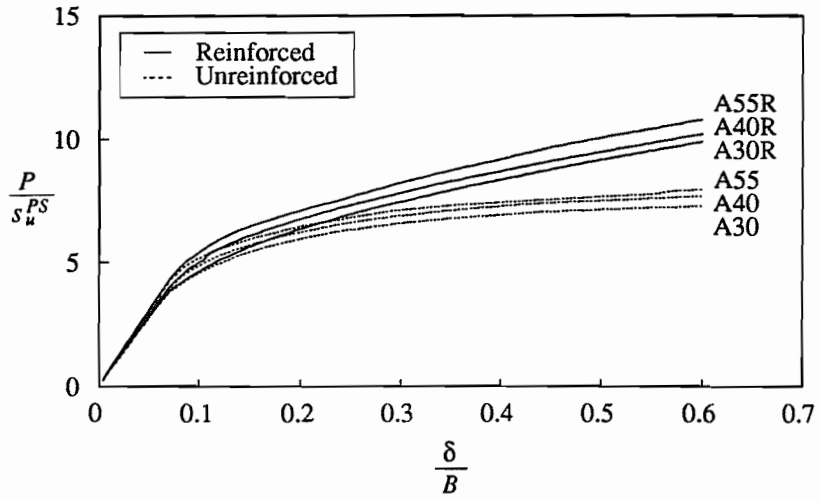

A) D_f = 0.15 *m*

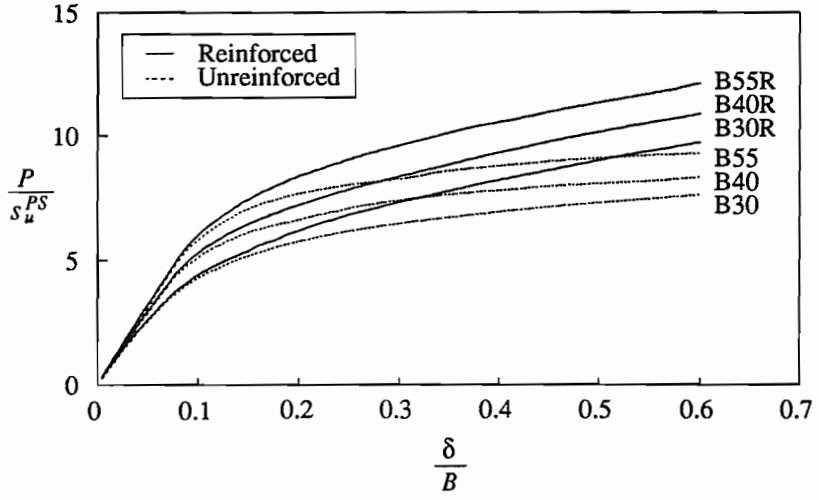

B) D_f = 0.30 *m*

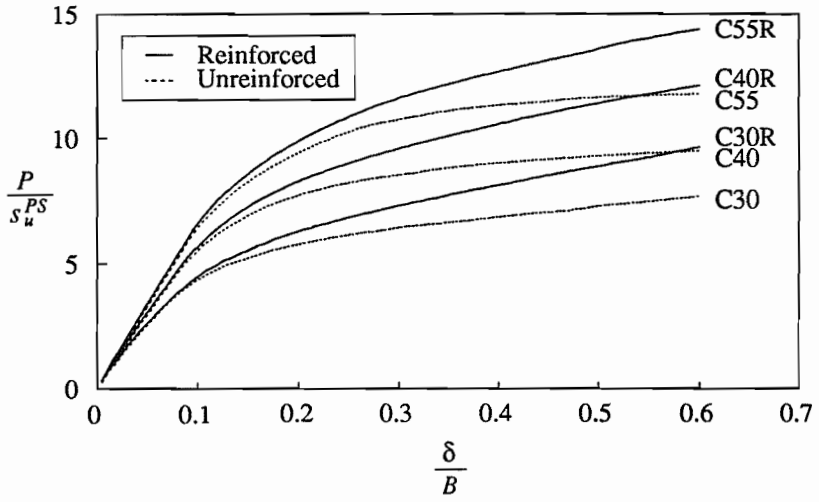

C) D_f = 0.50 *m*

Figure 7.1: Pressure-Displacement Responses for Different Fill Depths (D_f) and Friction Angles

UNREINFORCED						REINFORCED						
F.E.				Analytical		F.E.				Analytical		
Ref.	$\frac{P_f}{s_u^{PS}}$	β °	δ_f °	Ref.	$\frac{P_f}{s_u^{PS}}$	Ref.	$\frac{P_f}{s_u^{PS}}$	β °	δ_f °	Ref.	$\frac{P_f}{s_u^{PS}}$	$\frac{F_r}{B\, s_u^{PS}}$
A30	7.23	37.2	-7.7	RA30	4.78	A30R	9.87	35.0	-7.7	RA30R	7.30	2.13
A40	7.64	37.4	-6.2	RA40	5.72	A40R	10.18	36.4	-7.2	RA40R	7.42	1.61
A55	7.90	39.8	-7.0	RA55	6.56	A55R	10.76	41.6	-8.6	RA55R	7.88	1.29
B30	7.62	34.2	-5.3	RB30	5.39	B30R	9.72	34.3	-3.2	RB30R	9.35	2.95
B40	8.33	35.9	-8.0	RB40	6.56	B40R	10.86	40.9	-10.3	RB40R	10.49	3.28
B55	9.28	42.6	-12.3	RB55	8.65	B55R	12.11	43.6	-15.8	RB55R	11.02	2.86
C30	7.70	37.2	-0.1	RC30	7.97	C30R	9.63	34.1	+8.1	RC30R	10.28	0.69
C40	9.52	48.3	-7.1	RC40	11.80	C40R	12.10	45.3	-4.3	RC40R	15.53	3.48
C55	11.79	58.8	-12.8	RC55	18.38	C55R	14.38	56.7	-13.4	RC55R	20.80	3.70

Table 7.2: Final Footing Pressures (P_f / s_u^{PS}), Load Spread Angles (β), Footing Base Friction Angles (δ_f) and Analytical Reinforcement Forces ($F_r / (B\, s_u^{PS})$)

From the finite element results presented in Figure 7.1 and Table 7.2 it is clear that increasing the fill strength increases the load bearing capacity of the two-layer soil structure for both the unreinforced and reinforced cases. The amount of improvement in P_f obtained by increasing ϕ_{PS} from 30° to 55° is greater for the thicker fill layer ($\approx 50\%$ improvement for $D_f = 0.5\ m$), compared to the thinner layer ($\approx 9\%$ improvement for $D_f = 0.15\ m$). These percentages of improvement, due purely to the increased fill strength, appear to be independent of whether the system is unreinforced or reinforced. However, the actual presence of reinforcement has more effect for the thin fill layers than for the thick layers, an average of 35% strengthening is achieved by including reinforcement for $D_f = 0.15\ m$, compared to the 25% average improvement for $D_f = 0.5\ m$. Clearly, for large fill thicknesses a greater amount of benefit maybe obtained by increasing the fill strength, than is acquired by including reinforcement, but for thin fill layers the reverse applies.

Increasing the fill depth from 150 *mm* to 500 *mm* has a small effect on the bearing capacity of the two-layer soil system for unreinforced weak fills ($\approx 6\%$ improvement for $\phi_{PS} = 30°$), but an increased influence for increasing fill strengths ($\approx 49\%$ improvement for $\phi_{PS} = 55°$). Interestingly, in the reinforced analyses increasing the thickness of the weak fill actually reduces the bearing capacity slightly ($\approx -2\%$), although positive improvements are made for the stronger fills ($\approx 34\%$ improvement for $\phi_{PS} = 55°$). Evidently increasing the fill depth significantly increases the bearing capacity for fills of medium strength and above, in this case for $\phi_{PS} \geq 40°$.

For an increase in D_f the calculated angles of friction at the base of the footing, δ_f, generally tend to increase (and similarly the outward acting footing frictional forces) for the stronger fill strengths, but for medium ϕ_{PS} they remain comparatively constant and for the weaker fills δ_f decreases. Furthermore, this trend is somewhat exaggerated by the presence of reinforcement to the extent that the analysis of the reinforced thick weak fill (run C30R) develops an inward acting footing frictional force, $\delta_f = +8.1°$, which significantly reduces the analytical reinforcement force.

Comparing the finite element results of P_f, given in Table 7.2, to the equivalent analytical solutions, it is apparent that the finite element predictions are larger for the thin

fill, but for medium D_f they are about equal (or a little higher) and for thick D_f the finite element results are smaller than the analytical. This discrepancy between the finite element and analytical results is particularly noticeable for the analytical runs RC55 and RC55R. The differences in P_f between the finite element and analytical results is a direct consequence of the erroneous assumption made in the Houlsby *et al.* (1989) method of a constant uniform distribution of normal stress within the load spread area at the fill base. The actual upper interface normal stress distributions (shown in Figure 7.4) vary substantially, and are more spread out for $D_f = 0.5\ m = 2.0B$ than for $D_f = 0.15\ m = 0.6B$, which consequently produces larger values of load spread angle (by the 95% limit method) and therefore gives spuriously high values of analytical P_f for the thicker fills. It is noteworthy that for the thick weak fill analysis (RC30R) the analytical method actually predicts a bearing capacity type failure of the fill, because of the large β value.

The variations in the load spread angle (β) for increases in the fill strength and fill depth are presented in Table 7.2 and shown in Figures 7.2 a) and b) respectively. The load spread angle is extremely variable with ϕ_{PS} and D_f, but interestingly it is relatively insensitive to the presence of reinforcement. In Figures 7.2 a) and b) β increases only slightly with an increasing ϕ_{PS} for $D_f \leq 1.2B$ (i.e. the increase between β_{A30} and β_{A55} is only 7%), but for $D_f > 1.2B$ then β is a strong function of the friction angle (i.e. the increase between β_{C30} and β_{C55} is 58%).

These variations in β for changes in D_f and ϕ_{PS}, observed in the finite element analyses, can be compared to those variations seen in the experimental tests of Love (1984) and to those variations predicted by the bearing capacity theory proposed by Meyerhof (1974).

Love (1984) recorded measurements of the area along the clay surface effected by the footing load (which is an indication of the load spread angle), for different fill thicknesses, in his experimental two-layer soil tests. The total effective footing width on the clay ($2B'$) was defined as the distance along the clay surface between stationary points in the displacement vector plots. These measurements and the related load spread angle, derived by equation (7.2), are presented in Table 7.3 for each D_f (where B is the footing half width = 37.5 *mm*).

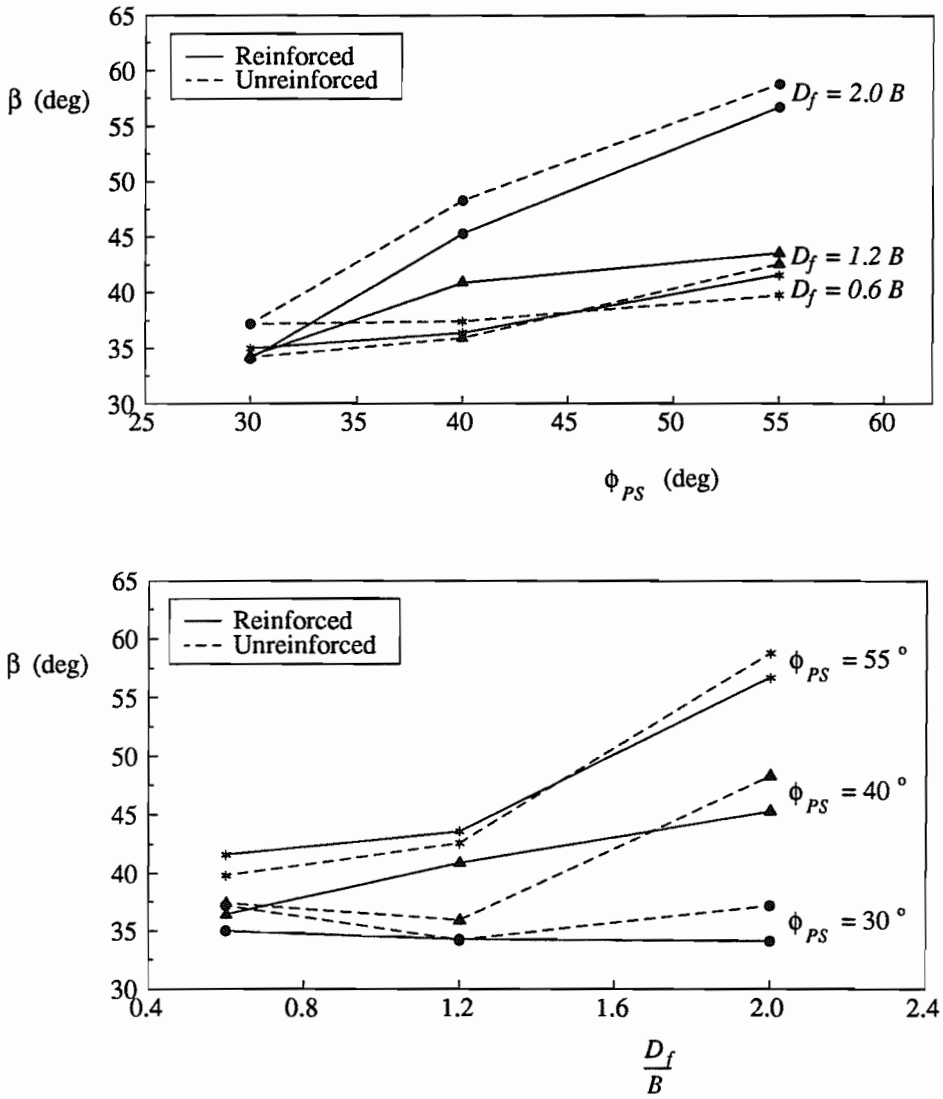

Figure 7.2: Variations of Load Spread Angle, β, with a) Plane Strain Friction Angle, ϕ_{PS} ; b) Fill Depth, D_f

Burd (1986) back-analysed the experimental tests by Love (1984) and established a best fit friction angle of $\phi_{PS} = 36°$. With reference to Figure 7.2 a), a friction angle of 36° would be expected to give an increasing β for increasing values of $D_f > 1.2\,B$. However, the experimentally determined β values in Table 7.3 seem to be insensitive to the fill depth and, moreover, consistently higher for the reinforced case compared to the unreinforced case, unlike the numerically established load spread angles. This difference of the variations in β for changes in D_f, with and without reinforcement, is because Love (1984) interpreted the length B' from the measured displacements within the clay, whereas the finite element β in Table 7.2 is calculated from the computed normal stress distributions within the fill.

		Reinforced			Unreinforced		
		Nominal Clay Strength (kPa)					
		6	9	14	6	9	14
$D_f =$	$4B/3$	124 (26.1°)	110 (19.3°)	108 (18.3°)	105 (16.7°)	105 (16.7°)	97 (12.4°)
	$2B$	134 (21.5°)	132 (20.8°)	137 (22.5°)	110 (13.1°)	129 (19.8°)	129 (19.8°)
	$8B/3$	163 (23.7°)	153 (21.3°)	142 (18.5°)	139 (17.7°)	139 (17.7°)	130 (15.4°)

Table 7.3: Values of $2B'$ (mm) and (β), estimated from equation (7.2), at a Footing Penetration of 25 mm = $2B/3$ (After Love (1984))

$$\beta = \tan^{-1}\left\{\frac{B' - B}{D_f}\right\} \tag{7.2}$$

Clearly, the load spread angle, which is only a convenient simplification of the real loading situation anyway, is highly sensitive to the particular method of interpretation. However, it should be noted that the experimental β, in Table 7.3, does tend to reduce with increased clay strength, which is an important relationship discussed further in Chapter 10.

Meyerhof (1974) predicted the ultimate bearing load (F_u), of a strip footing resting on a dense sand layer overlying soft clay, to be:-

$$F_u = 2B(\pi+2)s_u^{PS} + 2P_p \sin\delta \tag{7.3}$$

where B is the footing half width and P_p is the total passive earth pressure, inclined at an average angle δ acting upwards on a vertical plane through the footing edge, Figure 7.3.

The failure surface in the fill was originally thought to be of a logarithmic spiral shape (Meyerhof (1974)), but this was later modified to a more uniform truncated pyramidal shape by Hanna and Meyerhof (1980), which is assumed here to have a constant inclination of β from the vertical, as shown in Figure 7.3.

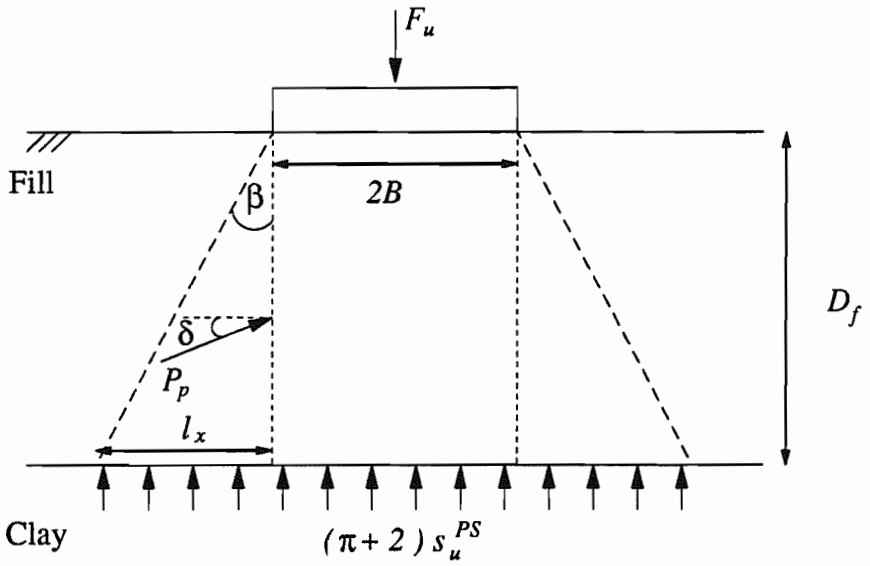

Figure 7.3: Failure of Soil below Footing on Dense Sand above Soft Clay (After Meyerhof (1974))

The total passive earth pressure is given by Meyerhof (1974) as:-

$$P_p = \frac{\gamma_f D_f^2 K_s \tan\phi_{PS}}{2\sin\delta} \tag{7.4}$$

where K_s is the coefficient of punching shearing resistance on the vertical plane through the footing edge, determined from the corresponding earth pressure coefficients, and γ_f is the unit weight of the fill.

By force equilibrium it is shown that:-

$$P_p \sin\delta = l_x (\pi+2)\, s_u^{PS} \tag{7.5}$$

where l_x is the horizontal distance, along the clay surface, between the boundary of the load spread area and the vertical plane through the footing edge (see Figure 7.3).

Thus, by substituting equation (7.4) into equation (7.5), the assumed load spread angle, β, is given by:-

$$\tan\beta = \frac{l_x}{D_f} = \frac{P_p \sin\delta}{(\pi+2)\, s_u^{PS} D_f} = \frac{\gamma_f D_f K_s \tan\phi_{PS}}{2(\pi+2)\, s_u^{PS}} \tag{7.6}$$

This new relationship in equation (7.6), derived from the Meyerhof (1974) theory, does not predict the correct β angles as given in Table 7.2, but it does show how β varies with the fill depth, fill friction angle and clay strength. The coefficient K_s is shown by Meyerhof (1974) to increase rapidly with ϕ_{PS}. Thus, the variations in β can be tabulated as:-

By equation (7.6)	Finite Element	Love (1984)
β increases with increasing D_f	YES (for $\phi_{PS} \geq 40°$)	NO
β increases rapidly with increasing ϕ_{PS}	YES (for $D_f > 1.2\,B$)	-
β reduces with increasing s_u^{PS}	YES (Chapter 10)	YES

Table 7.4: Variations of β by Theoretical, Numerical and Experimental Analyses

7.3.2 Normal Stress Distributions

The distributions of normal stress (σ) along the unreinforced and reinforced interfaces of the eighteen different two-layer soil systems listed in Table 7.1, are shown in Figure 7.4, where σ is non-dimensionalised by the plane strain, undrained, clay shear strength (s_u^{PS}) and the distance from the centre-line (x) is non-dimensionalised by the footing half width ($B = 0.25\ m$). The range of calculated load spread angles (β) for changes in fill strength, at a particular fill depth, are also given within Figure 7.4.

For each of the unreinforced runs the normal stresses at the centre-line are calculated as $5.5\ s_u^{PS}$ for $D_f = 0.6\,B$ and $5.7\ s_u^{PS}$ for $D_f \geq 1.2\,B$ approximately, which is between 5% and 7% more than the ultimate bearing capacities, given by $(\pi + 2)\ s_u^{PS} + \gamma_f D_f$, for each fill depth. This small amount of additional peak loading, above the ultimate bearing capacity, is believed to be a consequence of the peripheral load distribution outside of the established load spread area, as described in Section 6.3.5 and Figure 6.13.

For unreinforced thin fills σ maintains a relatively constant distribution within the loaded area independent of the friction angle, but as D_f increases the distribution becomes

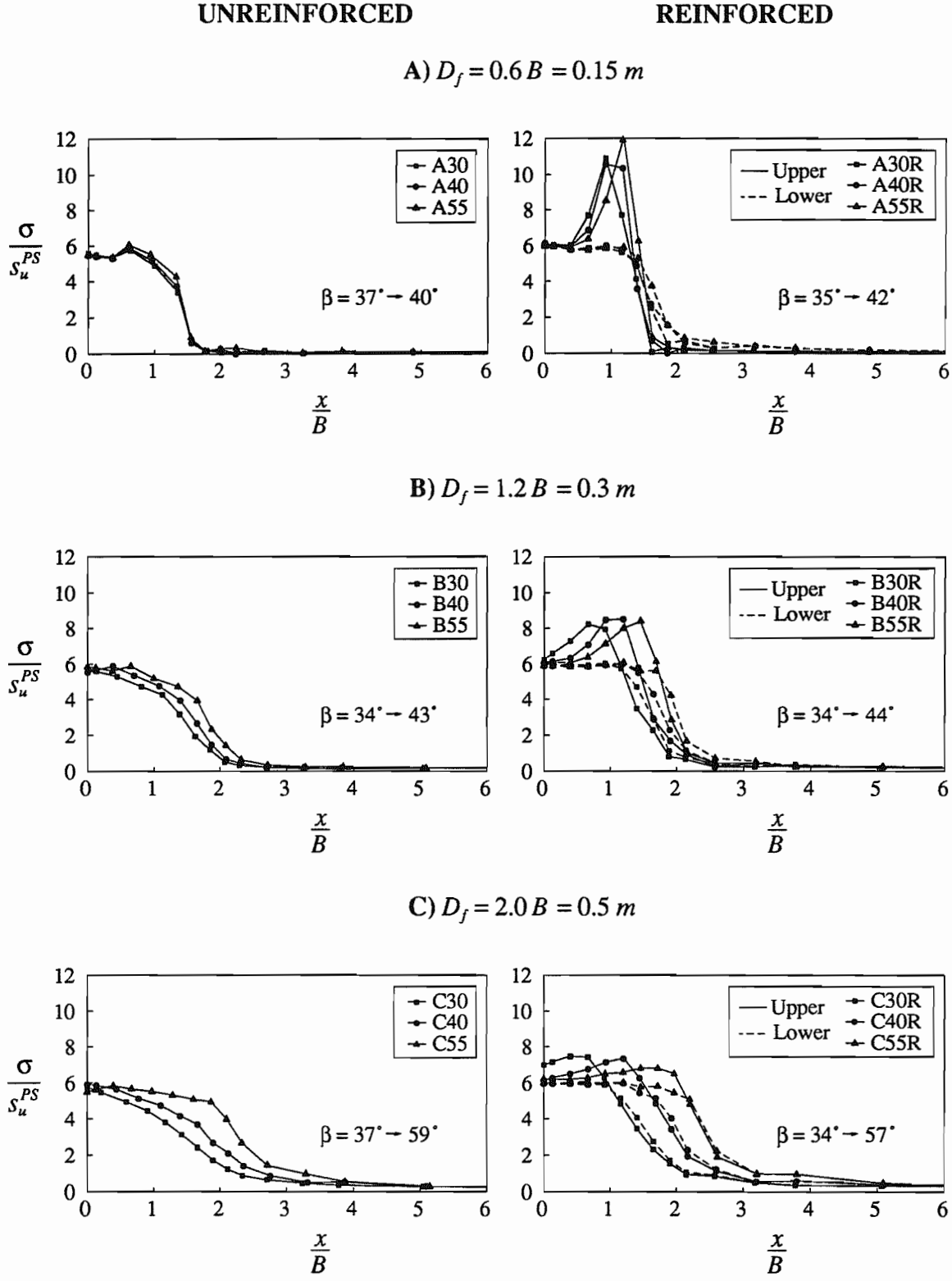

Figure 7.4: Normal Stress (σ / s_u^{PS}) along Interface for Varying Fill Depths (D_f) and Friction Angles, (at $\delta = 0.6B$)

increasingly spread out by an amount that depends on the friction angle, (seen particularly clearly for $D_f = 0.5\ m$). This is because of the presence of large outward acting shear stresses (illustrated in Figure 7.5) which reduce the normal stresses, particularly for the thicker fill.

The total normal force acting at the unreinforced interface and the area of the load spread, both increase for increasing ϕ_{PS} and as the fill depth increases this effect becomes even more appreciable, i.e. the normal force for run A55 is 6% greater than for run A30, while for run C55 the normal force is 33% greater than for run C30. This is the same effect as seen in the pressure-displacement responses, Figure 7.1.

In the reinforced analyses the lower normal stress distributions each begin on the centre-line at approximately $6\ s_u^{PS}$, which is due to the increased load capacity of the clay created by the inward acting shear stresses (Figure 7.5) outside of the vertically loaded area (Figure 6.16 Mode 2). The lower normal stresses maintain a more uniform distribution within the load spread area, in comparison to the equivalent unreinforced analyses, as predicted by plasticity theory. The extent of the load spread area increases for increasing ϕ_{PS} and for increasing D_f , as in the unreinforced cases. The normal stress distributions on the upper reinforcement surface are different from those on the lower surface, especially for the thin fill thickness, but this effect reduces for increasing D_f where the upper normal stresses reach progressively smaller maximum peak values, i.e. the effect of reinforcement on the normal stresses is much more distinctive for the thin fills than for the thick fills. Clearly, the large displacement reinforcement mechanisms, such as the tensioned membrane mechanism, contribute less to the overall reinforcing effect as the fill depth increases, whereas the small displacement mechanisms, such as changes in load spread angle, contribute more.

7.3.3 Shear Stress Distributions

As with the normal stresses, the distributions of shear stress, τ , along the unreinforced and reinforced interfaces are shown in Figure 7.5.

UNREINFORCED **REINFORCED**

A) $D_f = 0.6B = 0.15\ m$

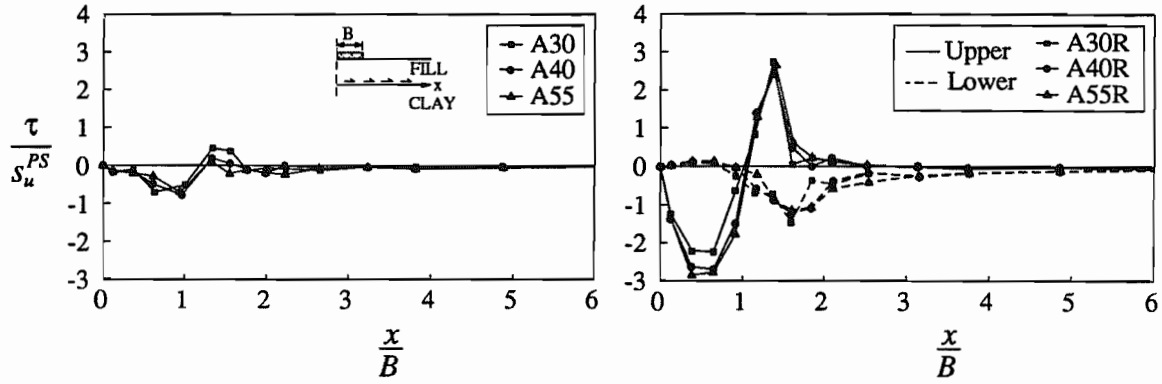

B) $D_f = 1.2B = 0.3\ m$

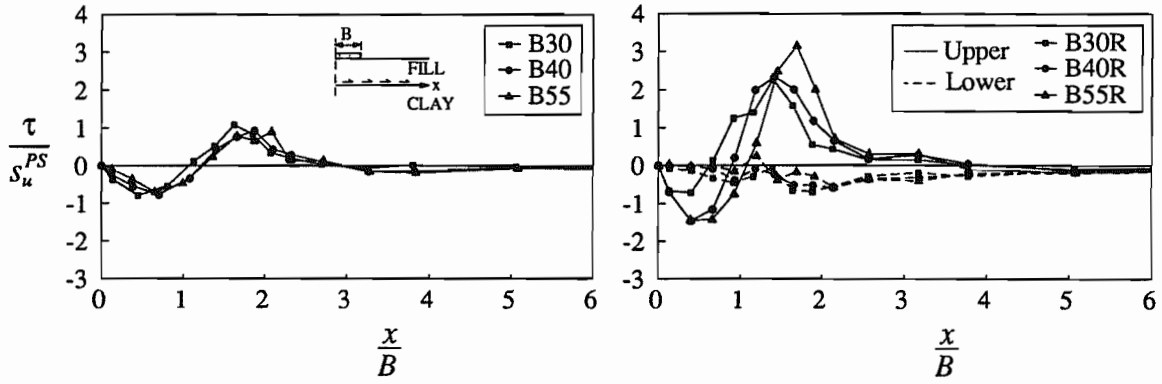

C) $D_f = 2.0B = 0.5\ m$

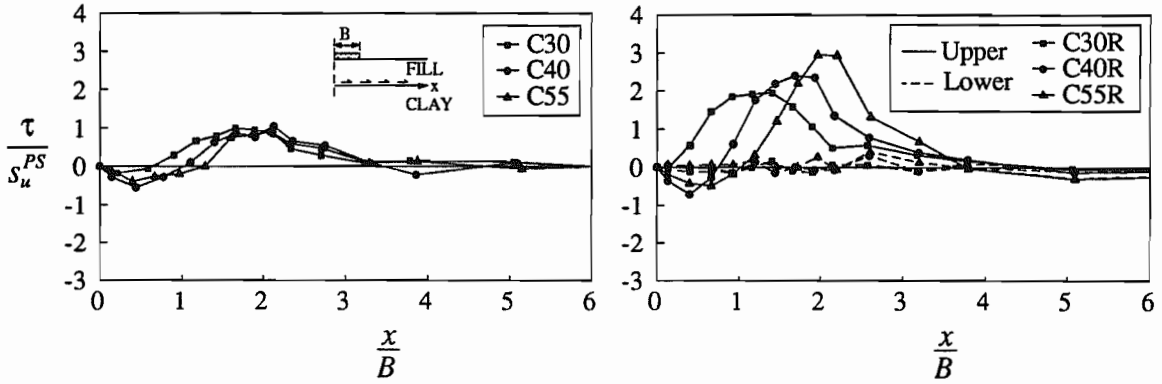

Figure 7.5: Shear Stress (τ / s_u^{PS}) along Interface for Varying Fill Depths (D_f) and Friction Angles, (at $\delta = 0.6B$)

For the unreinforced analyses inward acting shear stresses of about -0.8 s_u^{PS}, maximum, develop directly under the footing for $D_f = 0.15\ m$, but as the fill depth increases these reduce significantly. These inward shear stresses, within the vertically loaded area, do not contribute globally to the bearing capacity of the clay, but are significant in that they contradict the assumption in the analytical method, which predicts large outward acting shear stresses. At approximately $x = 1.2\,B$ the shear stresses reverse direction and as D_f increases these outward acting stresses become greater (peak $\tau \approx 1\ s_u^{PS}$) and distribute across a larger area before finally diminishing to zero. It is these large outward shear stresses, away from the loaded area beneath the footing, that are responsible for the reduction in the normal stresses, i.e. the shear stress effect.

In the reinforced analyses the shear stresses on the lower reinforcement surface are virtually insignificant directly under the footing regardless of the fill depth. However, further along the clay surface τ becomes quite a large inward acting stress for the thin fill layer ($D_f = 0.15\ m$) reaching a peak of $\approx -1.2\ s_u^{PS}$ beyond the load spread (greater than s_u^{PS} because of the discretization error, as explained in Section 5.4.5), which improves the load bearing capacity of the clay by approximately 11% (Figure 6.16). As D_f increases these inward clay shear stresses diminish and remain relatively small throughout the interface length, illustrating the reduced shear stress mechanism of the reinforcement for thick fills.

The shear stress distributions on the upper reinforcement surface for $D_f = 0.15\ m$ vary between large inward acting ($< -2\ s_u^{PS}$) under the footing, to large outward acting ($> 2\ s_u^{PS}$). As D_f increases the inward shear stresses reduce considerably, leaving only the outward shear stresses acting on the upper reinforcement surface.

A feature of all the unreinforced and lower reinforced shear stress distributions shown in Figure 7.5 is that they are relatively unaffected by variations in the fill strength, ϕ_{PS}. However, the upper reinforced shear stress distributions tend to both increase in outward acting peak value and to shift further along the reinforcement, away from the footing centre-line, for an increase in ϕ_{PS}, which is an effect that becomes more pronounced with increasing fill thickness.

7.3.4 Reinforcement Tension Distributions

The distribution of tension in the reinforcement, F_r, along its length is shown in Figure 7.6 for each fill depth.

With increasing variations in the fill strength, the peak reinforcement tensions increase marginally and shift slightly away from the footing centre-line. This effect becomes more exaggerated with decreasing D_f, but the more prominent feature seen in Figure 7.6 is that the centre-line tension increases appreciably as both the fill layer thickens and ϕ_{PS} decreases. This is because the magnitude of the outward shear force applied by the fill increases as D_f increases and it moves nearer to the footing centre-line as ϕ_{PS} reduces (Figure 7.5). Consequently the reinforcement sustains a greater amount of force, in the area directly under the footing, as D_f increases.

The maximum reinforcement tensions predicted using the Houlsby *et al.* (1989) analysis, Table 7.2, are lower than the peak tensions shown in Figure 7.6, and are, in fact, better approximations of the centre-line tensions. It is suggested that the reason for this is two-fold. Firstly, outward shear stresses act on the underside of the reinforcement for distances of up to $5B$ from the footing centre-line (Figure 7.5). This results in a build up of reinforcement force with distance towards the footing centre-line. For the case of $D_f = 0.6\,B$ this results in a tension of about 1.9 (non-dimensional units) at $x = 2\,B$. At this point the outward acting shear stresses, on the upper reinforcement surface, combine to produce a peak tension of about 4.0 units. It is the tension associated purely with these outward acting shear stresses (in this case about 2.1 units) which should be compared with the limit-equilibrium results (in this case 2.13 units for $\phi_{PS} = 30°$). This particular example is a very good agreement, although the comparison gets slightly worse with increasing friction angle. For the thicker fill, $D_f = 2.0\,B$, the lower shear stresses are very small and do not significantly contribute to the reinforcement tension, consequently the analytical predictions are within just 3% of the peak finite element values of F_r, except for run RC30R, which is because of the large inward footing friction force. Secondly, the Houlsby *et al.* (1989)

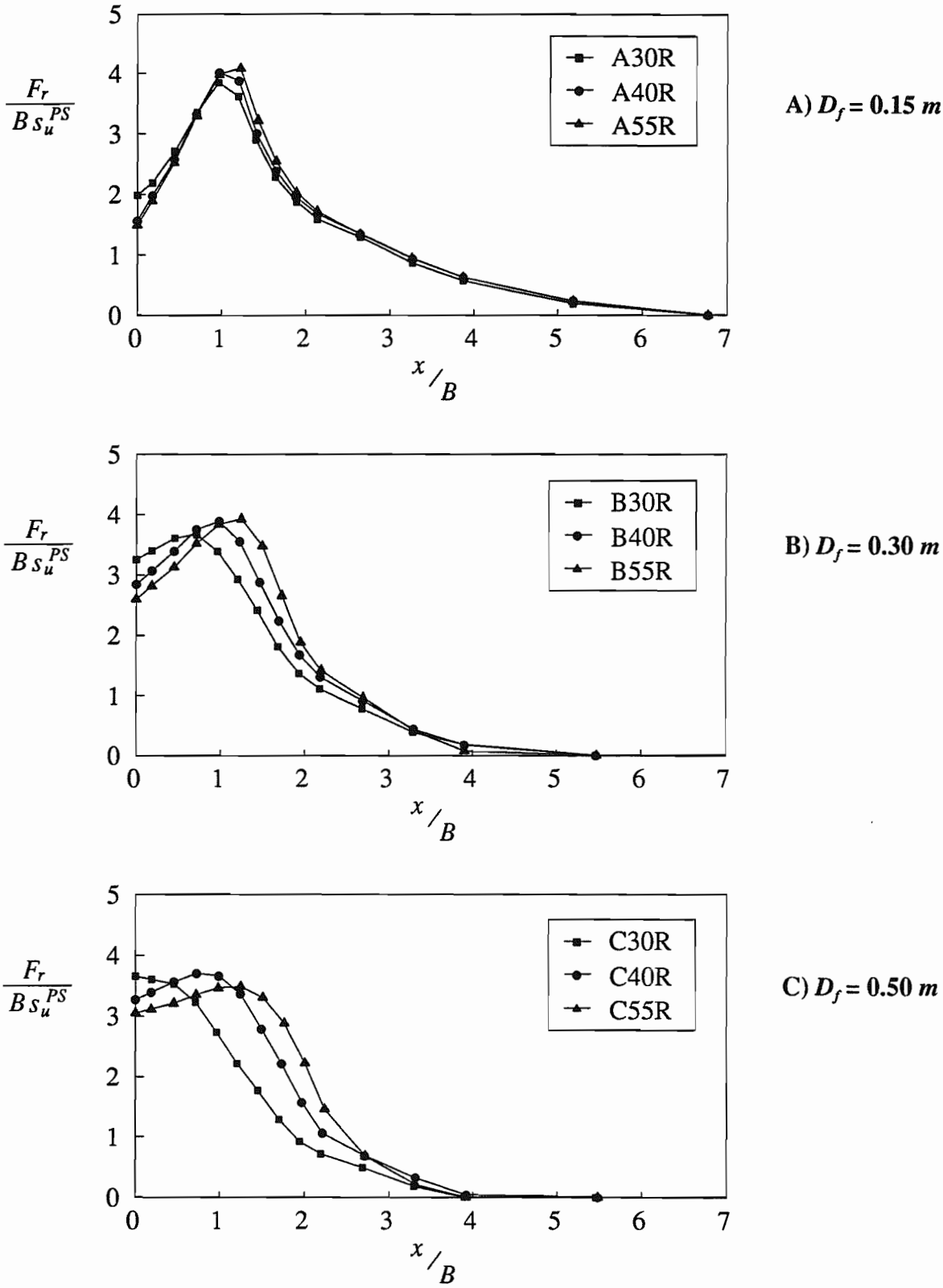

Figure 7.6: Reinforcement Tension (F_r / ($B\ s_u^{PS}$)) for Different Fill Depths (D_f) and Friction Angles, (at $\delta = 0.6\,B$)

method for calculating tensions due to fill shear stresses is non-conservative, it assumes that the fill is in a state of active failure beneath the footing when generally it is not, as discussed in Section 6.5.6.

7.3.5 Slip and Deformation along Interfaces

The relative slip, u_r, along the unreinforced and the upper and lower reinforced interfaces is shown in Figure 7.7, for each fill depth and strength. As D_f increases, the magnitude of the slip decreases for all fill strengths. The reinforced analyses, however, maintain higher values of u_r, compared to the unreinforced due to the higher footing loads. In the unreinforced cases there is a small amount of negative slip directly below the footing, where the clay is moving out (away from the footing centre-line) from under the fill layer, which creates inward acting shear stresses on the clay surface as shown in Figure 7.5. However, beyond about $x = 1.5\,B$ the fill begins sliding out over the clay (positive u_r) creating outward shear stresses which reduce the clay bearing capacity factor, N_c. This mode of positive slip is sustained over a large distance for the thick fill layer, whereas for the thinner layers the relative slip reverses direction again, but does not generate any significant shear stresses because the normal stresses are small, Figure 7.4.

In the reinforced cases the upper interfaces are subjected initially to negative u_r and therefore inward shear on the reinforcement, due to the clay dragging the reinforcement outwards, for all fill thicknesses and strengths. However, between approximately $x = 1.5\,B$ and $3\,B$ the fill slides out over the reinforcement, generating outward upper shear stresses, Figure 7.5. Concurrently the lower reinforcement interfaces experience negative slip (i.e. inward shear on the clay) as the clay flows away from the centre-line, an effect which diminishes to zero for the thick fill.

The final deformed profiles of the unreinforced and reinforced interfaces are plotted in Figure 7.8. The presence of reinforcement changes the profiles appreciably only in the area of reversed curvature, by reducing the amount of upward heave. As D_f increases, the amount of vertical displacement at the centre-line reduces slightly ($\approx 3\%$ for $D_f = 2\,B$), for unreinforced and reinforced. The noticeably lower centre-line displacements for runs C30 and C30R are the consequence of a bearing capacity type failure operating in the fill.

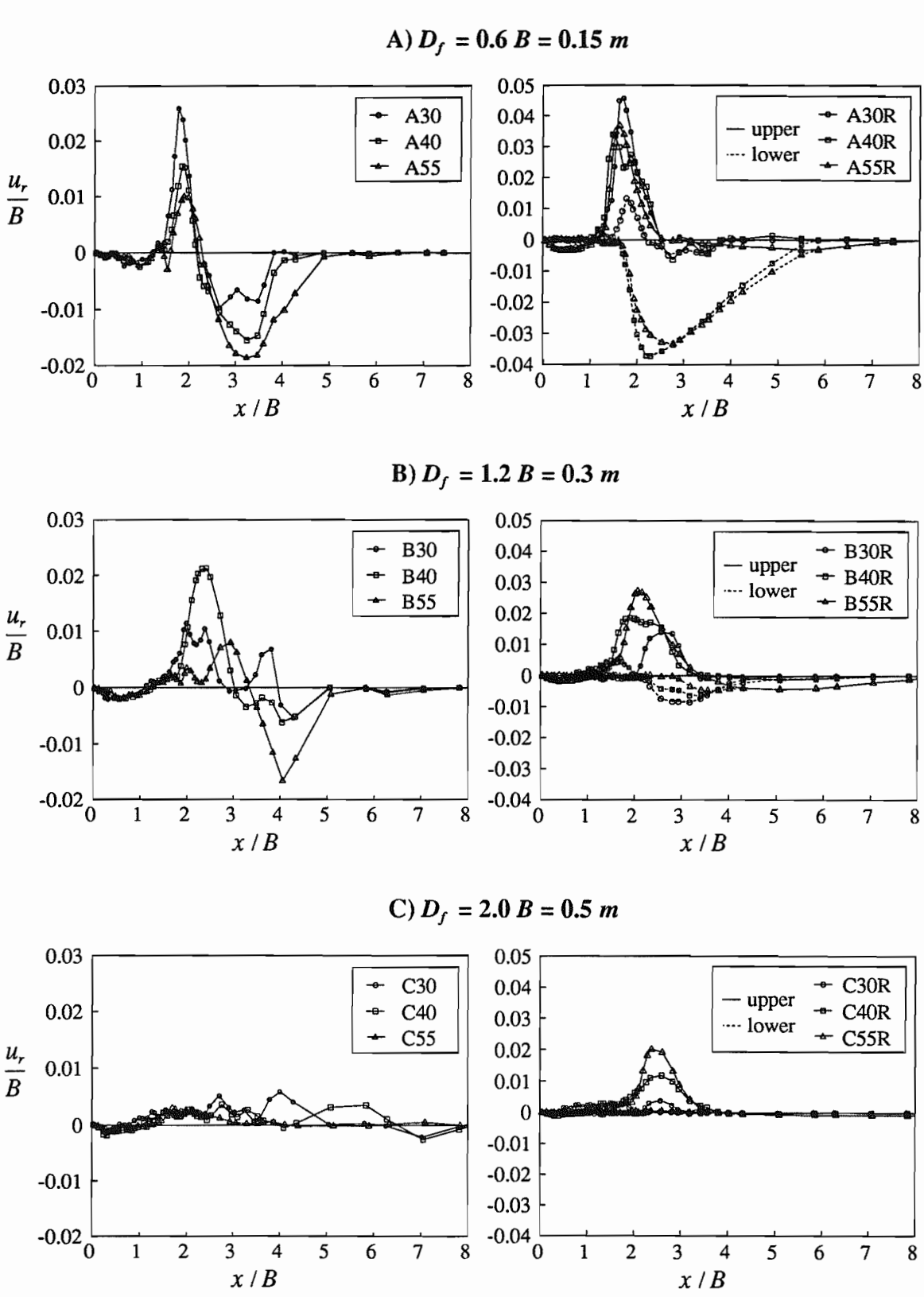

Figure 7.7: Relative Slip (U_r) along the Interfaces

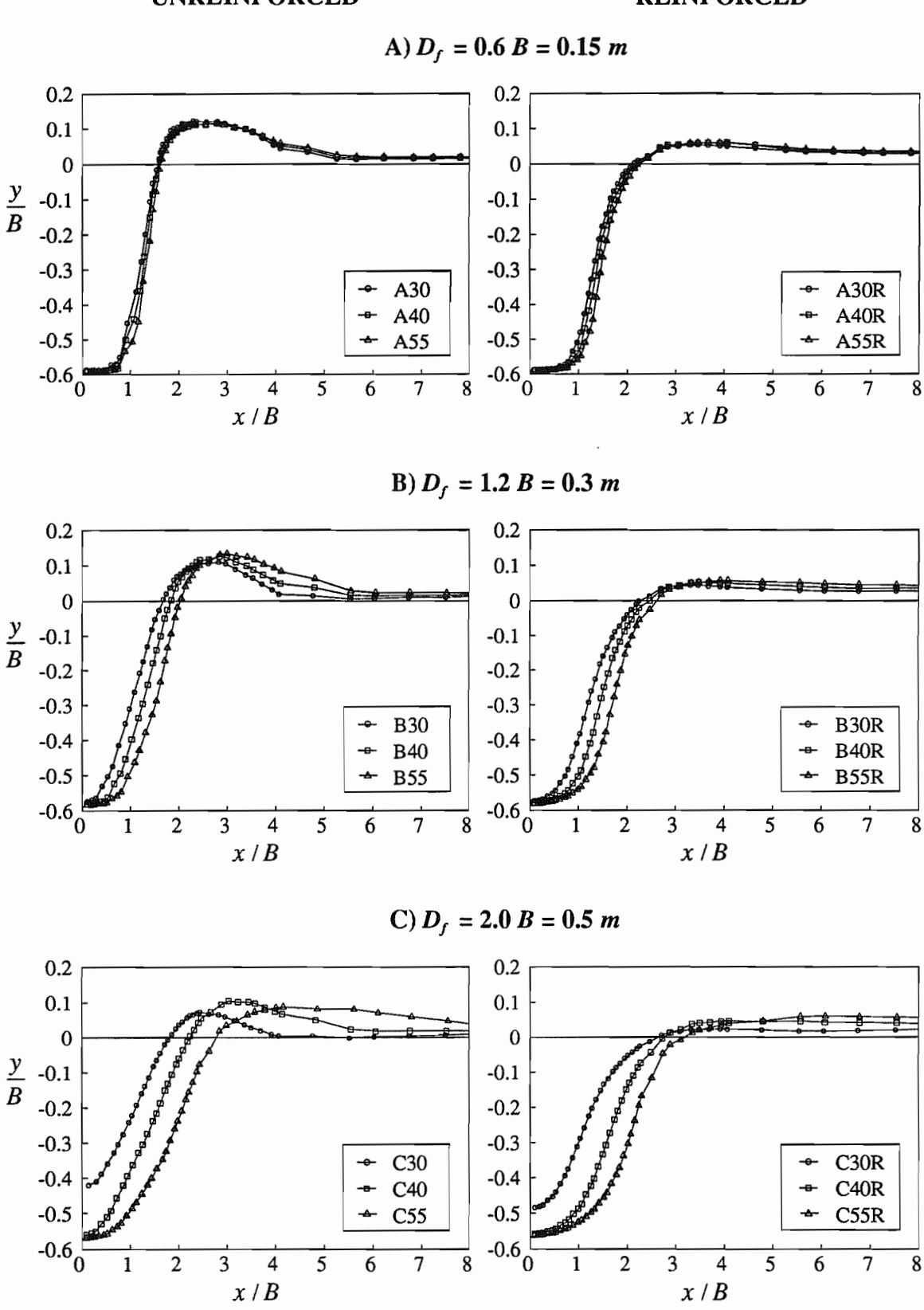

Figure 7.8: Final Deformed Shape of the Interfaces

7.4 General Conclusions

The effect of reinforcement seems to be greater for thin fills than for thick fills. The pressure-displacement responses, Figure 7.1, show that for a fill depth of $0.6B$ the effect of reinforcement is very marked, whereas increasing the fill friction angle has little effect. For thick fills ($D_f = 2B$) changes in the friction angle have a much greater effect than including reinforcement. This also shows up well in the distributions of the normal stress, Figure 7.4. At large values of D_f it may be more effective to increase ϕ rather than to use reinforcement (although the presence of reinforcement may, indirectly, improve compaction and hence ϕ).

The normal stress plots illustrate well the effect of increasing the fill thickness on the width of the loaded area on the clay surface. For thin fills the stresses drop sharply to zero at a point that is roughly independent of friction angle. For thick fills, however, the normal stress distributions are more smooth and extend laterally by an amount that depends on the fill friction angle. This aspect of the results leads to considerable difficulties in interpreting the results using simple load spread type models. Firstly, the diffuse nature of the normal stresses for thick fills results in a value of β which, when used in a conventional load spread analysis, gives loads that are too large (Table 7.2). Secondly, the value of any load spread parameter clearly varies with fill thickness and friction angle in a way that is difficult to quantify. A compromise might be to suggest that a simple load spread analysis might be suitable for, say, $D_f < B$, for thicker fills a different analysis would need to be adopted.

Investigating the normal stresses at the interface of the reinforced two-layer soil system illustrates the reduced role of the large displacement reinforcement mechanisms, such as the tensioned membrane, and the increased role of the small displacement mechanisms, such as a larger load spread area, which occur as the fill depth increases.

CHAPTER 8:

INFLUENCE OF REINFORCEMENT STIFFNESS

8.1 Introduction

The plethora of reinforcement materials that are currently available to design engineers is continually increasing. There is a large variety of different materials, such as polymer grids and synthetic fabrics, each designed to offer different physical capabilities, such as strength, interlock, separation, porosity, transmissivity, etc., depending upon the particular requirement. Naturally this has resulted in the materials possessing a wide range of different stiffnesses, for example Tensar materials have a stiffness of between 350 kN/m to 730 kN/m , whereas Bidim materials have typically between 800 kN/m and 2 000 kN/m stiffness. Clearly the stiffness of a geosynthetic material is an important property to consider when designing reinforced two-layer soil structures subjected to footing loads.

The design procedures currently in use for two-layer soil systems are generally based on the use of simple analytical models of behaviour to calculate the response of the structure to a single load application, with the extension for the case of repeated loading made on the basis of empirical correlations, as discussed in the literature review. These design procedures, in general, develop a series of mathematical equations which can be used to assure stability of the two-layer soil system. A large number of variables are introduced into the design equations in an attempt to model accurately the various materials involved. The stiffness of the geosynthetic reinforcement is one such commonly used design variable, see Nieuwenhuis (1977), Giroud and Noiray (1981), Sowers *et al.* (1982), Giroud *et al.* (1984), De Groot *et al.* (1986), Sellmeijer *et al.* (1982), and Sellmeijer (1990). However,

it is not a parameter considered in all of the currently used design methods, for instance Houlsby *et al.* (1989) and Houlsby and Jewell (1990), where the inherent assumption is made that the geotextile stiffness is sufficient to provide 'full reinforcement'.

The purpose of this study is to decide whether the concept of 'full reinforcement' is useful and if so, how stiff the reinforcement needs to be in order to achieve it.

8.2 Parametric Study

This study is based on four large displacement plane strain finite element calculations using the 'central parametric analysis' and the material properties given in Appendix 6A, with a variety of reinforcement stiffnesses.

The reinforced 'central parametric analysis' (run B40R) possesses a reinforcement stiffness of 300 kN/m, which is typical of a proprietary polymeric geogrid material. Geosynthetic membranes of stiffnesses 30 kN/m (run B40A) and 3 000 kN/m (run B40C) would be thought of as being 'flexible' and 'stiff' respectively. The equivalent unreinforced two-layer soil system (run B40) is also included in the study.

The small displacement Houlsby *et al.* (1989) analytical predictions equivalent to the unreinforced and reinforced finite element 'central analyses' are presented for comparison.

8.2.1 Load-Displacement Response

The footing pressure-displacement responses for each of the four large strain finite element runs and the two 'central' comparative analytical predictions, are illustrated in Figure 8.1, where P is the average value of vertical stress beneath the footing and δ is the vertical footing displacement. The full set of results are presented in Table 8.1, where 'U' signifies the unreinforced and 'R' the reinforced analytical calculations.

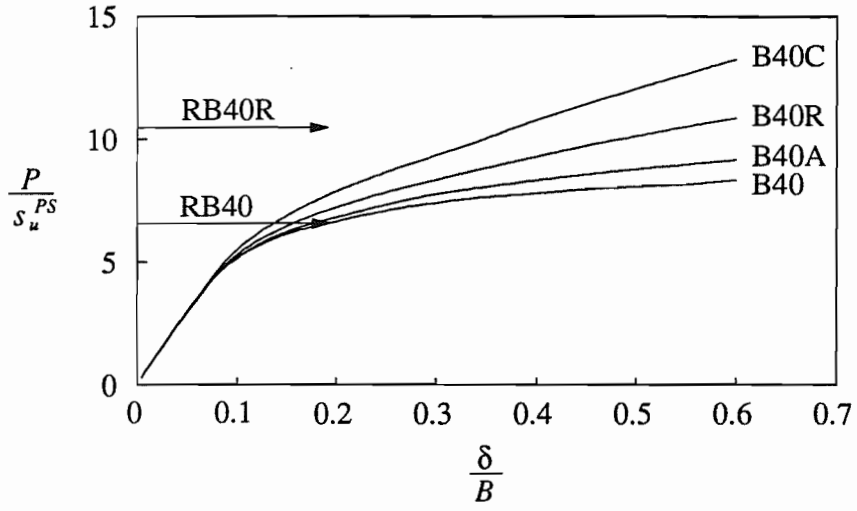

Figure 8.1: Pressure-Displacement Response for Different Reinforcement Stiffnesses (J)

F.E.					Analytical			
Ref.	J	P_f / s_u^{PS}	δ_f	β	**Ref.**	J	P_f / s_u^{PS}	$F_r / (B\ s_s^{PS})$
B40	0	8.33	–8.0°	35.9°	RB40	U	6.56	-
B40A	30	9.17	–9.8°	37.1°	RB40A	R	9.81	3.02
B40R	300	10.86	–10.3°	40.9°	RB40R	R	10.49	3.28
B40C	3000	13.24	–7.8°	36.7°	RB40C	R	9.74	2.65

Table 8.1: Run References for the Finite Element and Analytical Results Shown in Figure 8.1

Clearly the reinforcement has little influence on the elastic behaviour of the system, but an increasing influence as the footing displacement increases and plastic soil deformations start to occur. At footing displacements larger than $\delta = 0.1\,B$ a greater improvement in the load bearing capacity of the system is obtained in-line with the increased stiffness of the reinforcement. The gradients of the pressure-displacement curves for the reinforced runs, increase with reinforcement stiffness due to the 'tensioned membrane' effect, where the tensions in the reinforcement combine with the membrane curvature to

reduce the normal stresses applied to the subgrade (illustrated in Figure 8.2), thus increasing the footing load for a given footing displacement. This effect increases with increasing footing displacement and reinforcement stiffness.

The amount of improvement in the final footing pressure P_f at $\delta = 0.6\ B$, acquired through increasing the stiffness of the reinforcement, is not proportional to the actual stiffness value. Incorporating a flexible reinforcement with a stiffness of 30 kN/m (B40A) increases the load by 10% above the unreinforced capacity. Increasing the stiffness tenfold increases this improvement to 30%, and a further tenfold stiffness increase takes this figure to 60%. Clearly the increase in load capacity is not proportional to the stiffness and is a case of diminishing returns, suggesting that the use of very stiff reinforcement material in two-layer soil systems is unlikely to be economical. Furthermore, this contradicts the theory of any analytical methods which predict a linear relationship between the value of reinforcement stiffness and the bearing capacity improvement, e.g. Giroud and Noiray (1981) and Sowers *et al.* (1982).

The analytical method underestimates P_f for the unreinforced case (RB40), because it predicts a large contribution by the footing frictional force to the assumed outward acting shear stresses at the base of the fill layer, when in fact the shear stresses are inward acting in the area beneath the footing (Figure 8.2). For the cases with a flexible (RB40A) and a moderately stiff (RB40R) reinforcement the analytical predictions of the final footing pressures are reasonably comparable to the finite element values, with less than a 6.5% difference. However, the analysis for the stiff reinforcement (RB40C) substantially under-predicts P_f , because the Houlsby *et al.* (1989) method does not consider the influence of the large displacement tensioned membrane mechanism, which becomes significant for this high stiffness case, Figure 8.2.

8.2.2 Normal and Shear Stress Distributions

The normal (σ) and shear (τ) stresses, extracted from the appropriate interface element Gauss points, that are acting along the upper and lower reinforcement surfaces at the final footing displacement of $\delta = 0.6\,B$ are plotted in Figure 8.2.

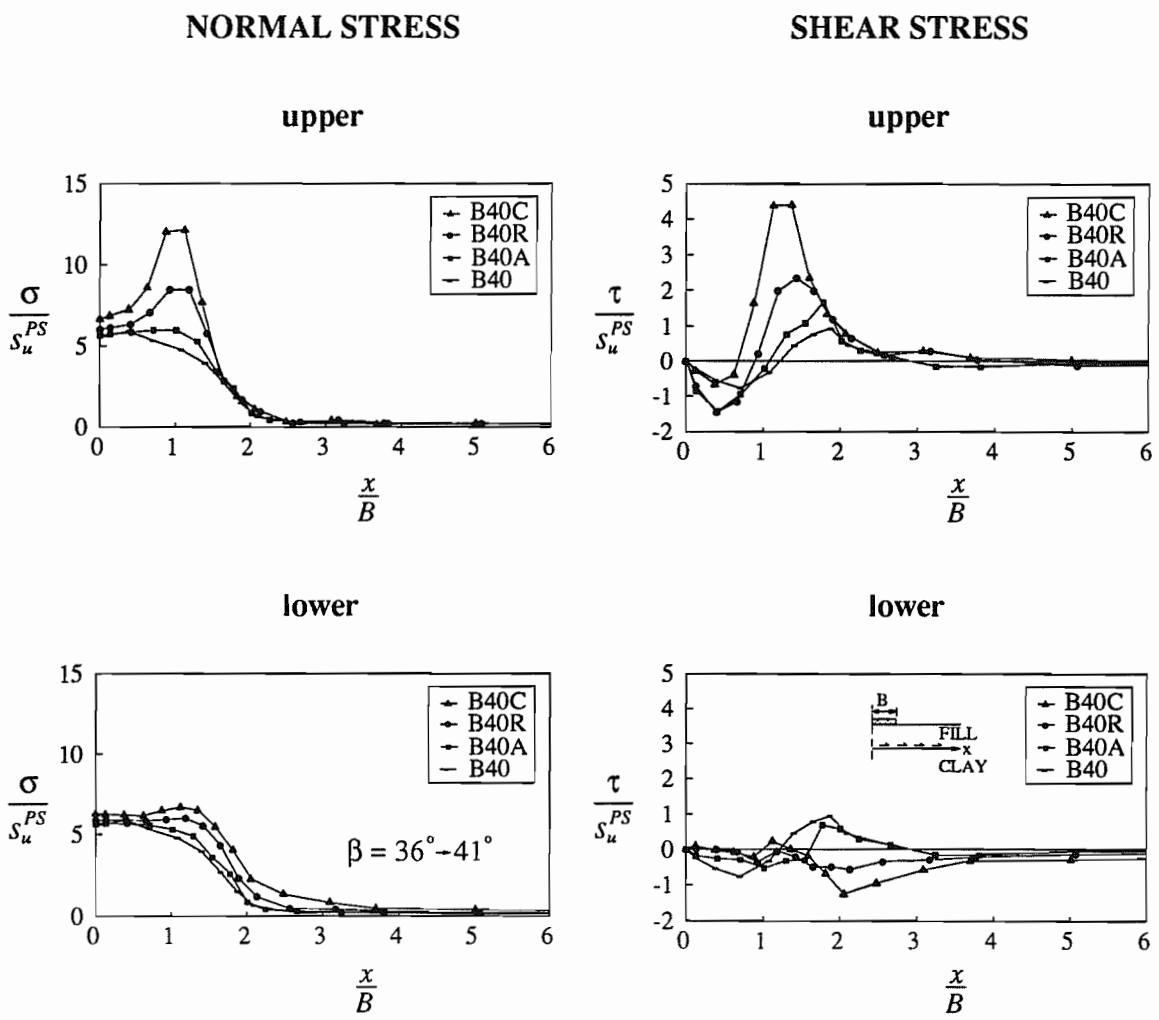

Figure 8.2: Normal Stress (σ / s_u^{PS}) and Shear Stress (τ / s_u^{PS}) along Interface for Varying Reinforcement Stiffnesses (J), (at $\delta = 0.6\,B$)

Comparison of the upper and lower surface normal stress distributions indicate that within the area of approximately $x = 0$ to $1.5\,B$ the reinforcement is subjected to different magnitudes of normal stress. This difference in σ is due to the tensioned membrane effect which increases with the reinforcement stiffness. The magnitude of the normal stresses

acting on the subgrade immediately beneath the footing is approximately constant and it is suggested that in this region the clay is being subjected to a bearing capacity type failure. If no shear stresses were acting on the clay surface then the magnitude of the normal stresses in this region would be expected to be a constant value of $(\pi + 2)\, s_u^{PS} + \gamma_f D_f$ as given by equation (6.3). However, the presence of the outward acting shear stresses has the effect of reducing the normal stresses, particularly for the runs B40 and B40A.

The shear stress distributions along the upper reinforcement surface show that for each value of reinforcement stiffness the outward shear stresses induced by the fill on the reinforcement reach a peak at a horizontal distance x of about $1.5\,B$ from the footing centre-line and that as the reinforcement stiffness increases then the magnitude of these shear stresses also increases. It is suggested that this effect is caused partly by the greater total footing load, which is needed to achieve $\delta = 0.6\,B$, and partly by the reinforcement constraining the base of the fill from displacing laterally by an amount that increases as the reinforcement stiffness increases. This fill restraint mechanism, discussed in Chapter 2, thus causes an increase in the lateral stresses induced at the top of the fill, as seen in the plots of the principal stress directions, Figures 8.6.

Similar increases in shear stress at the upper reinforcement interface, for increases in reinforcement stiffness, where found by Hird and Kwok (1989) and (1990). They propose that high lateral stresses develop near the top of the fill embankment due to its "bending" or "arching", comparable to Figure 8.6 b). Which, for a very high reinforcement stiffness (i.e. 15 000 kN/m), become excessively large, leading to an increase in the upper interface shear stresses and hence the total reinforcement force.

The shear stress distributions along the lower reinforcement surface, immediately beneath the footing, show that the clay subgrade is subjected to a small amount of inward acting stress for all values of reinforcement stiffness. However, for values of x greater than $1.5\,B$ the shear stresses for the unreinforced case (B40) and the flexible reinforcement case (B40A), reverse direction and become significant outward acting stresses ($\tau_{peak} \approx 1\, s_u^{PS}$) which reduce the normal stresses acting on the clay at failure (refer to Figure 6.16 Mode 4). These detrimental outward shear stresses arise from the transmission of shear stresses at the

base of the fill, highlighting the inadequacy of very flexible membrane materials. For the stiffer reinforcements the clay layer is subjected to inward acting shear stresses almost throughout, i.e. the beneficial 'shear stress mechanism' of the reinforcement. The magnitudes of these inward shear stresses increase with increasing reinforcement stiffness, which is caused by the reinforcement restraining the clay as it endeavours to flow plastically away from the footing centre-line, see Figure 8.4.

There appears to be no significant change in the load spread angle (β) for increasing reinforcement stiffness, judging from the data in Table 8.1 and the plot of normal stresses at the fill base. However, there is an observed small improvement in the load distribution on the clay surface, but this does not contribute to the overall reinforcing effect to the same extent as the large displacement tensioned membrane mechanism.

The theory presented in the Houlsby *et al.* (1989) limit state design method assumes that none of the outward acting shear stresses at the base of the fill layer are transmitted onto the clay surface and that the entire reinforcement force is due solely to the fill shear stresses. It is also assumed that to achieve effective reinforcement the geotextile must be capable of providing a sufficient force at both ultimate capacity and small deformations, which will require the reinforcement to have a certain stiffness. However, it has been shown in the plots of shear stress distribution, Figure 8.2, that the shear stresses vary between inward and outward acting along the length of both the upper and lower membrane surfaces. Therefore, it can be assumed that the reinforcement tension is actually due to the sum of the shear forces that act on both the upper and lower surfaces of the reinforcement, which are found by integrating the shear stresses. This method of estimating the reinforcement force was used in the small strain finite element study of the influence of the reinforcement stiffness in two-layer soil systems, undertaken by Burd and Brocklehurst (1990). It was found that for low reinforcement stiffnesses, $< 60\ kN/m$, a proportion of the shear force induced by the fill was sustained directly by the clay, but as the reinforcement stiffness increased then the shear force in the clay reduced. However, for very large reinforcement stiffnesses, $> 3\,000\ kN/m$, the subgrade shear force began to increase, but acting inwards rather than outwards as it had for the smaller stiffnesses. This had the net result that the shear stresses at the reinforcement-clay interface continued to increase the force in the reinforcement.

8.2.3 Reinforcement Tension Distribution

The tensions generated in the reinforcement at the end of each calculation are plotted in Figure 8.3 in conjunction with the comparative analytical 'central' prediction, RB40R.

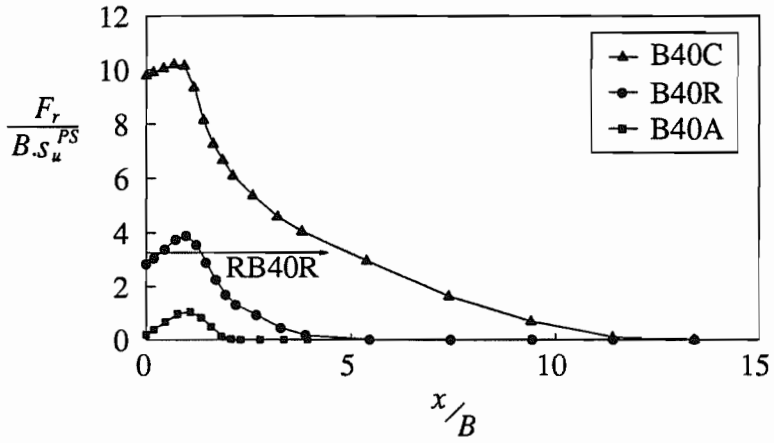

Figure 8.3: Reinforcement Tension ($F_r/(B\ s_u^{PS})$) for Different Reinforcement Stiffnesses (J), (at $\delta = 0.6\,B$)

An important feature of these results is that increasing the reinforcement stiffness causes a corresponding increase in the magnitudes of the forces induced in the reinforcement with only a small improvement in the footing pressure-displacement response, Figure 8.1. A similar result was also found in the Burd and Brocklehurst (1990) small strain reinforced two-layer soil system calculations for varying reinforcement stiffness.

Although the analytical values of the maximum reinforcement tension for the flexible (RB40A) and stiff reinforcements (RB40C), Table 8.1, are very different from the finite element results, because there is no consideration of the shear force applied to the reinforcement by the clay, the F_r value for the 'central' analysis is notably only slightly smaller than the peak value for run B40R, Figure 8.3.

8.2.4 Slip and Deformation along Soil-Reinforcement Interface

The relative slip, u_r, along the upper and lower reinforcement surfaces is illustrated in Figure 8.4 for each analysis. Positive slip indicates the upper interface surface moving to the right relative to the lower surface. As the reinforcement stiffness increases the magnitude of the upper relative slip increases also. Note the large amount of slip on the underside of the

reinforcement for run B40C, due to the clay flowing away from the centre-line, which generates the high inward shear stresses in Figure 8.2. Furthermore, the lower slip for run B40A is uncharacteristically positive at about $x = 2.3\,B$, because the reinforcement is not stiff enough to restrain the fill, causing outward shear stresses on the clay surface. The slip along the unreinforced interface is shown in Figure 6.23 a).

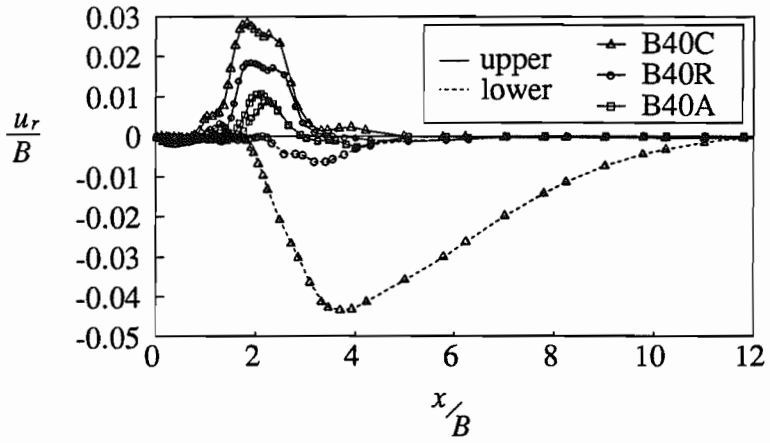

Figure 8.4: Relative Slip (u_r) along Interfaces

The final deformed profiles of the unreinforced and reinforced soil interfaces are shown in Figure 8.5. Clearly the reduction in the magnitude of the displacements at the interface for the reinforced cases, compared to the unreinforced case, is dependent upon the stiffness of the reinforcement. As J increases the membrane profile changes significantly, which contradicts the theory of any analytical methods which assume that the reinforcement maintains a constant deformed shape regardless of the reinforcement stiffness (e.g. the parabola assumed by Giroud and Noiray (1981)).

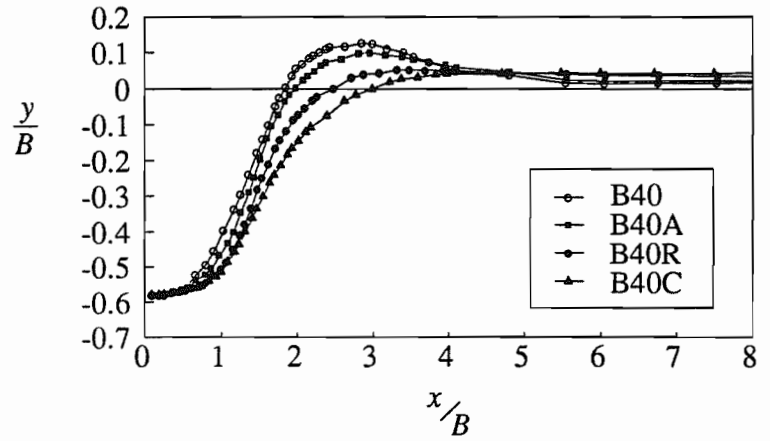

Figure 8.5: Final Deformed Shape of the Membrane

8.2.5 Principal Stress Directions

The principal stress directions in the fill layer for the flexible (B40A) and stiff (B40C) reinforcement analyses are plotted in Figure 8.6 and for the unreinforced (B40) and moderately reinforced (B40R) analyses in Figure 6.25 a). By comparing these figures it is evident that not only does the reinforcement cause a change in the principal stress directions, but also the magnitude of the principal stresses increases as the reinforcement stiffness increases, and an arching effect progressively develops beneath the footing.

Hird and Kwok (1989) and (1990) report that placing reinforcement at the base of an embankment can significantly reduce deformations in the foundation provided it is sufficiently stiff and strong, but that the benefit of increasing the reinforcement stiffness follows a "pattern of strongly diminishing returns". They conclude that for very stiff reinforcement the probability of arching in the embankment is increased, which would induce increased reinforcement force without any increase in stability of the fill. They predict that very little benefit is obtained by increasing the reinforcement stiffness beyond about 7 000 kN/m . Clearly, this same effect is also operating here, Figures 8.3 and 8.6.

8.3 General Conclusions

This large displacement parametric study suggests that increasing the reinforcement stiffness of a reinforced two-layer soil system can result in significant improvements in the load-displacement response of the footing, compared to that of an unreinforced system. A 60% greater final load capacity was achieved with a stiff reinforcement, compared to 10% improvement for a flexible one, at a footing displacement of 0.6 B . In contrast, the maximum improvement obtained with $J = 15\,000\ kN/m$ in a small displacement finite element calculation was only 15%, see Burd and Brocklehurst (1990).

As the reinforcement stiffness is increased the large displacement tensioned membrane mechanism provides an increasing contribution to the load improvement, whereas β remains relatively constant. However, for static loading there is little benefit to be gained from using excessively stiff reinforcement, since this generates an arching effect in the fill and induces large shear stresses between the soil and reinforcement, which do not in themselves contribute to an improvement in the static bearing capacity of the system and also give rise to large values of reinforcement force. It is possible, nevertheless, that these additional

stresses may improve the cyclic behaviour of the system. It seems probable that in practice the use of very stiff reinforcement is unlikely to be economical, for the returns gained in improved static loading capacity.

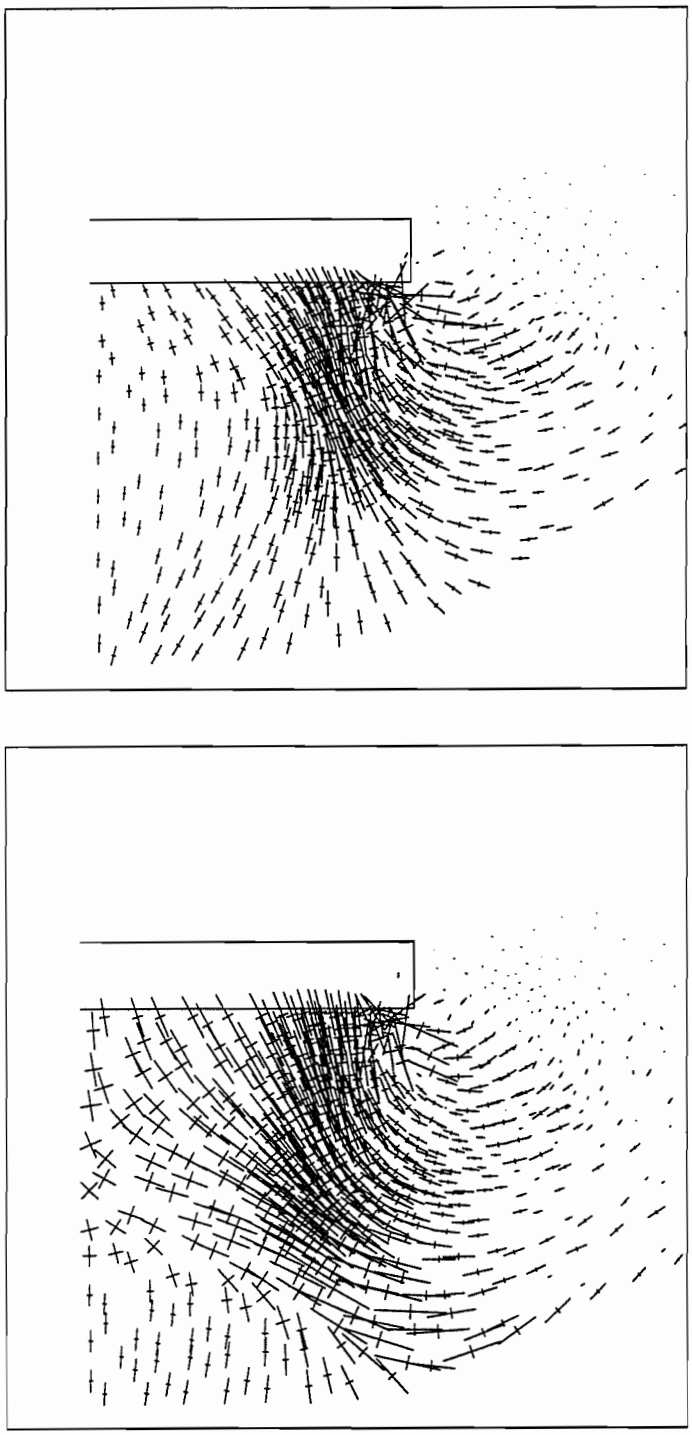

B40A

B40C

Figure 8.6: Principal Stress Directions in the Fill at $\delta = 0.6\,B$

CHAPTER 9:

INFLUENCE OF REINFORCEMENT LENGTH

9.1 Introduction

There are many analytical design methods for reinforced two-layer soils systems which advocate the need for membrane anchorage. The design methods either assume that the membrane is fixed at some arbitrary points beyond the load spread area, or stipulate that a minimum membrane length must be maintained outside of the area directly influenced by the load. This is so that simplifying assumptions can be made in order to calculate the tension in the membrane and hence the contribution of the tensioned membrane mechanism. The design methods and studies by Giroud and Noiray (1981), Giroud *et al.* (1984), Sellmeijer *et al.* (1982), De Groot *et al.* (1986), Bourdeau (1989) and Dembicki and Jermolowicz (1991), all specify membrane anchorage for the reasons which are elaborated upon below.

Giroud and Noiray (1981) and Giroud *et al.* (1984) determine the membrane curvature and hence estimate the reinforcement tension by assuming that the membrane is pinned at the limits of the loaded area. De Groot *et al.* (1986) describes a design method based on Sellmeijer *et al.* (1982) which specifies a required "anchorage length of geotextile" under the fill, over which the stress that has developed by the strain in the heavily deformed part of the membrane, will be reduced to zero due to friction on both sides of the geotextile. Bourdeau (1989) uses an iterative finite difference scheme to compute the tensile forces in the membrane by resolving both the vertical fill stress and the horizontal component of the frictional stress at the upper membrane interface. A minimum "active" length of

reinforcement is then evaluated to ensure full frictional anchorage such that the tension is zero at the free end. Dembicki and Jermolowicz (1991) calculate a minimum "length of anchorage", thought necessary to prevent slip at the reinforcement ends, by a force equilibrium equation which is dependent upon the fill-geotextile angle of friction and the coefficient of clay-geotextile adhesion, for a known maximum reinforcement tension.

However, from the results of the parametric study conducted in this chapter it is clear that the reinforcement does not need to be anchored to obtain an improvement in the structural performance of a two-layer soil system, nor indeed is it essential that the reinforcement covers any large width of the fill base.

9.2 Parametric Study

A facility exists within the finite element program OXFEM which allows certain reinforcement membrane elements to be prescribed a stiffness (J) of zero, while other membrane elements possess a real stiffness value, thus effectively changing the reinforcement length. Using this method, six large displacement plane strain finite element runs were completed with various reinforcement lengths (L) taken from the footing centre-line, Figure 9.1, using the finite element mesh B, Figure 5.2, and the material properties as given in Appendix 6A.

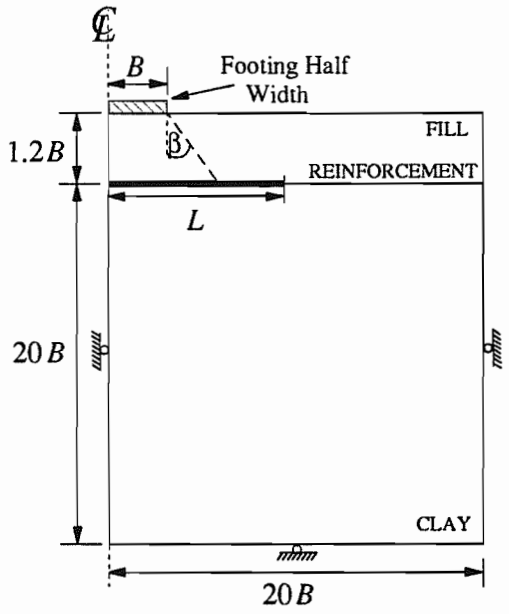

Figure 9.1: Simplified Cross Section of a Reinforced Two-Layer Soil System

9.2.1 Load-Displacement Response

The calculated footing pressure-displacement responses for each of the six finite element runs and the two 'central' analytical runs are shown in Figure 9.2 and the full set of results are presented in Table 9.1, where P is the average vertical footing pressure, δ is the vertical footing displacement, β is the load spread angle through the fill and δ_f is the angle of friction at the footing base.

The results of run B40R, with $L = 20\ B$, are listed in Table 9.1 so that they can be compared to those of run B40R5. However, the pressure-displacement response of run B40R is not plotted in Figure 9.2, because it is effectively identical to the response of run B40R5, as shown by comparing Figures 9.2 and 6.10.

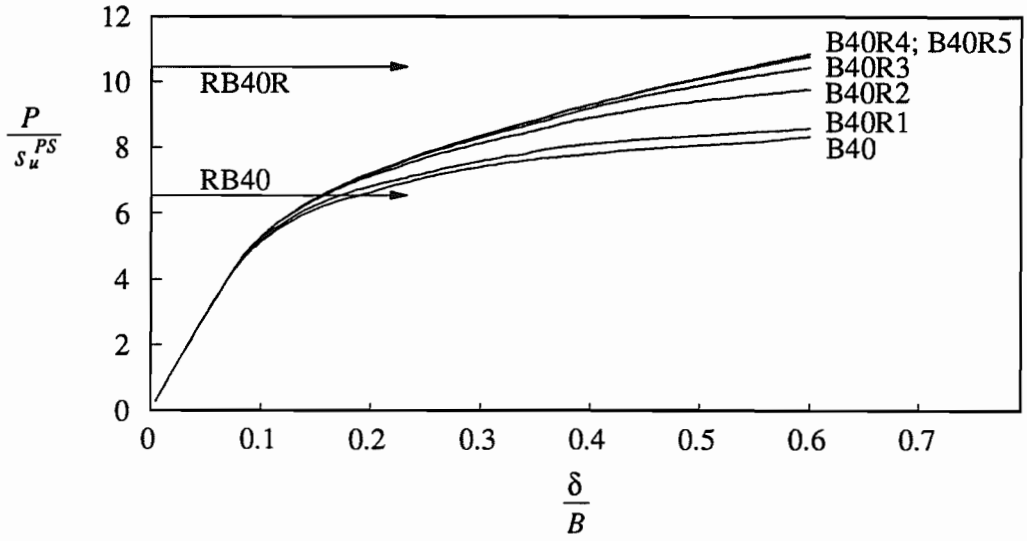

Figure 9.2: Pressure-Displacement Response for Different Reinforcement Lengths (L)

At footing displacements greater than $\delta = 0.1\ B$ there is an obvious divergence of the six load-displacement responses in Figure 9.2. The unreinforced and nominally reinforced ($L = 0.98\ B$) responses, runs B40 and B40R1, are very similar, indicating that this smallest of reinforcement lengths is completely inadequate as it does not cover the critical part of the subgrade surface that is affected by the imposed interface stresses, i.e. the bearing

F.E.					Analytical			
Ref.	L	P_f / s_u^{PS}	δ_f	β	**Ref.**	L	P_f / s_u^{PS}	$F_r / (B\, s_s^{PS})$
B40	0	8.33	−8.0°	35.9°	RB40	U	6.56	-
B40R1	0.98 B	8.57	−7.2°	34.0°	RB40R1	R	9.30	2.45
B40R2	1.47 B	9.77	−8.5°	37.0°	RB40R2	R	9.79	2.78
B40R3	1.96 B	10.45	−10.1°	42.4°	RB40R3	R	10.78	3.32
B40R4	2.8 B	10.78	−10.4°	44.4°	RB40R4	R	11.18	3.48
B40R5	4.0 B	10.86	−10.3°	40.9°	RB40R5	R	10.49	3.28
B40R	20.0 B	10.86	−10.3°	40.9°	RB40R	R	10.49	3.28

Table 9.1: Run References for the Finite Element and Analytical Results Shown in Figure 9.2

capacity of the clay, for both runs, is reduced because of the significant outward acting shear stresses that the clay sustains (illustrated in Figure 9.3). Furthermore, the length of reinforcement for run B40R1 is insufficient to build up shear stress.

For a reinforcement length of 1.47 B, run B40R2, there is some distinct improvement in the load bearing capacity, compared to runs B40 and B40R1. This length of reinforcement is sufficient to pick-up the majority of the detrimental shear stresses at the interface and to exhibit something of a tensioned membrane effect, but it is not capable of acting as an effective tensioned membrane when it is forced to deform at footing displacements greater than $\delta = 0.2\, B$. Whereas for the reinforcement lengths of $L \geq 1.96\, B$, runs B40R3, B40R4 and B40R5, the tensioned membrane mechanism operates successfully causing the footing pressures to increase with displacement at a fairly constant rate. An additional relatively small amount of increased footing load is obtained for each of the longer reinforcement lengths up to the maximum limit given by B40R5 (equivalent to run B40R).

It is clear from the results presented that a large improvement in the maximum applied footing load, compared to the unreinforced case, can be obtained by including reinforcement at the base of the fill ($\approx 30\%$ for B40R5), even though the membrane does not cover the

entire base area of the fill as was previously thought to be necessary. This contradicts the theory that firm anchorage of the membrane is essential to obtain adequate reinforcement. Similarly, this would be the case for reinforced unpaved roads, provided the wheel load followed a defined path and did not wander beyond the membrane area.

The reinforcement length cannot be adjusted specifically in the Houlsby *et al.* (1989) method, however the reinforced analytical predictions (presented in Table 9.1) give reasonable approximations to the finite element results with increases in the maximum footing pressure due to the increases in the estimated load spread angle. Whereas, the unreinforced analytical value of P_f is too low, because of the erroneous assumption of consistently outward acting shear stresses at the fill base, see Figure 9.3.

9.2.2 Normal and Shear Stress Distributions

Figure 9.3 shows the profiles of normal stress (σ) and shear stress (τ) along the length of the reinforcement at the final footing displacement of $\delta = 0.6\,B$.

The upper normal stress distributions show a progressive increase in the magnitude of the normal stresses acting on the reinforcement for increasing reinforcement length. As greater lengths of reinforcement are introduced the magnitude of the normal force applied by the fill increases gradually from the minimum in run B40, to the maximum in run B40R5. The normal stress distribution for run B40R5 can be seen to coincide with that for run B40R by comparing Figures 9.3 and 6.12.

The upper normal stresses for run B40 start at $\sigma = 5.43\,s_u^{PS}$ on the centre-line and after increasing only slightly diminish steadily to the residual self weight of the fill beyond about $x = 2.4\,B$. Whereas, for each increasing length of reinforcement, the centre-line normal stresses increase (up to a maximum of $\sigma = 6\,s_u^{PS}$ for B40R5), and a greater peak normal stress is reached due to the tensioned membrane effect. The difference in magnitude between these upper normal stress distributions is an indication of the different amounts of tensioned membrane effect acting in each reinforced two-layer soil system.

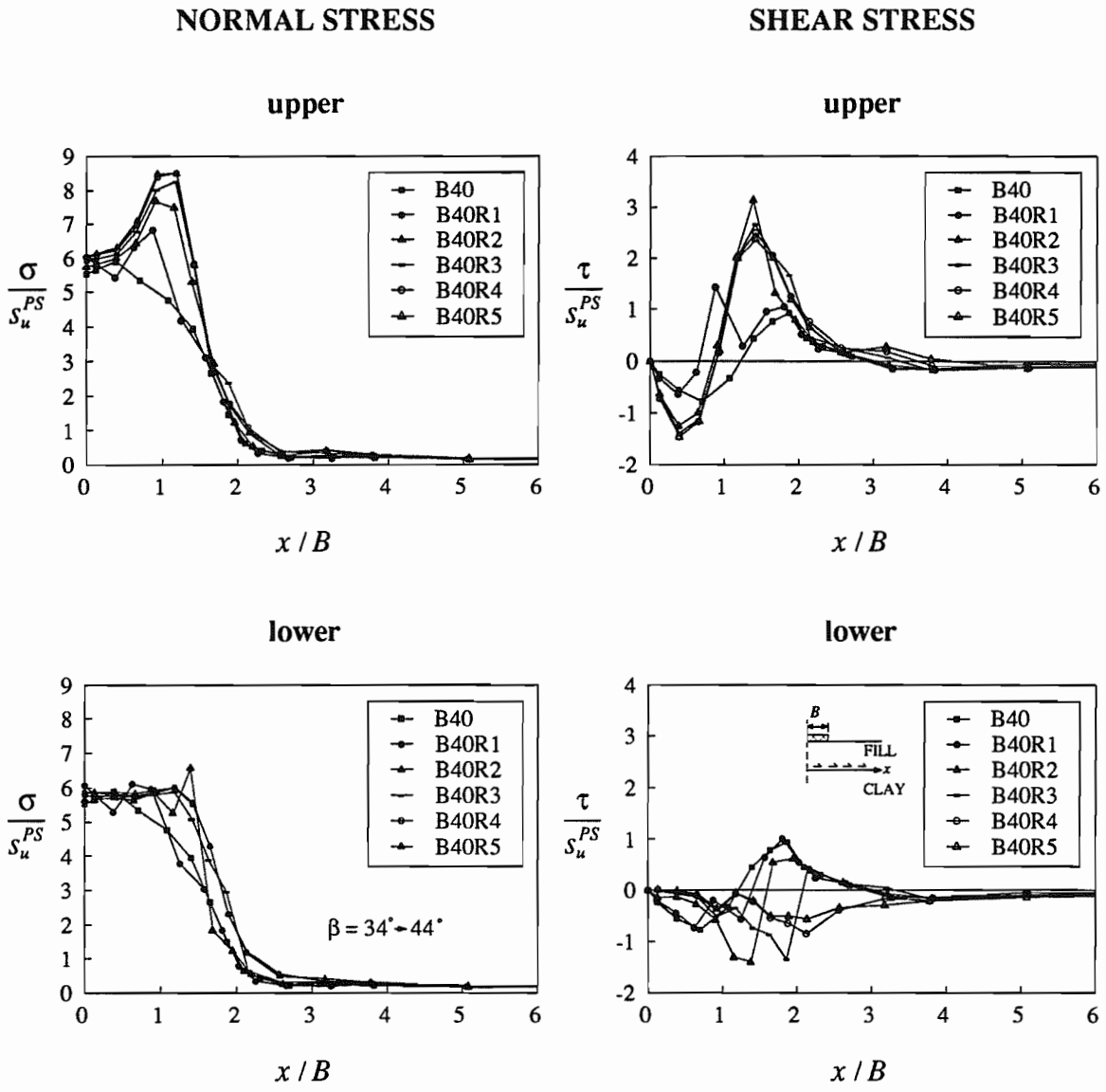

Figure 9.3: Normal Stress (σ/s_u^{PS}) and Shear Stress (τ/s_u^{PS}) along Interface for Varying Reinforcement Lengths (L), (at $\delta = 0.6\,B$)

The erratic nature of the lower normal stress profiles for runs B40R1 ($L = 0.98\,B$) and B40R2 ($L = 1.47\,B$) is caused by the abrupt ending of the reinforcement. The lower normal stress distributions are influenced by the outward acting shear stresses on the subgrade surface and for the unreinforced, B40, and nominally reinforced, B40R1, analyses especially, the normal stresses are noticeably reduced, at distances away from the centre-line, in comparison to the other runs. The runs B40R5, B40R4, B40R3 and to a degree B40R2,

approximately exhibit the theoretical uniform normal stress distribution with $\sigma \approx 5.9\, s_u^{PS}$, as estimated by equation (6.3) where $N_c = 1 + 3\,\pi / 2$ due to the inward acting shear stresses on the subgrade (Mode 2 in Figure 6.16).

From the plot of the lower normal stress distributions the small effect of an improved load spread is visible for the runs using reinforcement of an effective length (runs B40R5, B40R4 and B40R3), compared to those using an inadequate reinforcement length (runs B40, B40R1 and B40R2). The actual calculated load spread angles (β) are given in Table 9.1. However, the minor improvement in β does not contribute to the reinforcing effect as substantially as the tensioned membrane mechanism, which is a similar situation to that found during the investigation of the influence of increasing reinforcement stiffness (Section 8.2.2).

As L increases the pattern of the upper shear stress distributions along the length of the interface progressively changes as it converges to that of the adequately reinforced case, run B40R5. Directly under the footing the inward acting shear stresses increase from low stresses in run B40 ($\tau_{peak} = -0.7\, s_u^{PS}$) to high stresses in run B40R5 ($\tau_{peak} = -1.4\, s_u^{PS}$), and beyond $x = 1\,B$ they increase from comparatively small to much greater outward shear stresses. The horizontal distance at which the reinforcement ends in runs B40R1 and B40R2 is clearly defined by the sudden reduction in the outward shear stresses.

The distributions of shear stress on the lower reinforcement surface are rather unclear, but the trend is that for the unreinforced run B40 and nominally reinforced runs B40R1 and B40R2 the stresses transpose from inward to large outward acting ($\tau_{peak} = s_u^{PS}$) as x increases (which reduces the load bearing capacity as seen in Figures 9.2 and 9.3). While, for the more fully reinforced runs B40R3, B40R4 and B40R5, the distributions of shear stress almost entirely remain inward acting as x increases, except beyond the end point of the reinforcement in run B40R3 ($x = L = 1.96\,B$). The spurious peak inward acting shear stresses for runs B40R2 and B40R3, which exceed the shear strength of the clay, coincide with the end points of the different reinforcement lengths and are caused by discretization errors (see Section 5.4.5).

For this particular combination of two-layer soil properties and dimensions it is suggested that a reinforcement length of $L = 2\,B$ is sufficient to provide adequate reinforcement, since the tensioned membrane and shear stress mechanisms operate effectively. Note that there are still some diminishing shear stresses at the interface beyond $x = 2\,B$, which have an effect on the induced reinforcement force, see Figure 9.4.

9.2.3 Reinforcement Tension Distribution

Figure 9.4 shows that as the reinforcement length (L) increases, the force in the reinforcement (F_r) also increases throughout the membrane length, up to a maximum limit given by run B40R5 ($L = 4\,B$).

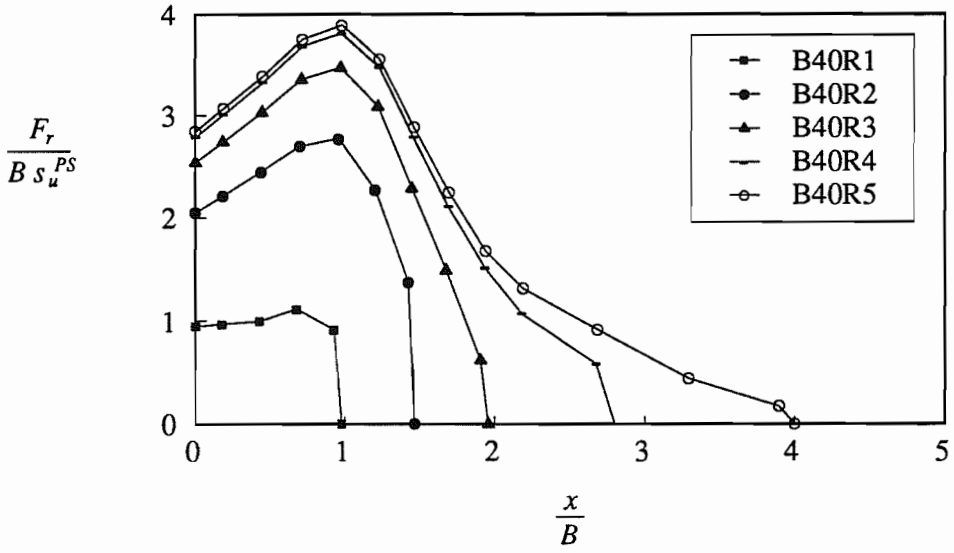

Figure 9.4: Reinforcement Tension ($F_r/(B\,s_u^{PS})$) for Different Reinforcement Lengths (L), (at $\delta = 0.6\,B$)

The reinforcement tensions obtained for runs B40R5 and B40R4 are virtually identical, but for run B40R3 ($L = 1.96\,B$) the tension is slightly smaller (10% lower at the peak value, where $x = 1\,B$), because L is not quite long enough to completely pick-up all of the force applied by the shear stresses at the interface beyond $x = 2\,B$. As a consequence of the even shorter reinforcement lengths in runs B40R2 and B40R1 their tension profiles are reduced still further. Clearly the smaller the reinforcement force, the less contribution the tensioned membrane mechanism can provide in reinforcing the system.

The analytical values of the reinforcement tension, Table 9.1, vary from the peak finite element results, Figure 9.4, because the clay shear forces are neglected. However, successively larger values of F_r are predicted due to the nominal increases in both the load spread angle and the outward acting footing frictional force, except for run RB40R5 which has a slightly lower value of β.

9.2.4 Slip and Deformation along Soil-Reinforcement Interface

The plots in Figure 9.5 of the upper and lower relative slip, u_r, for each reinforcement length are a little confused, because of the erratic oscillations in u_r at the reinforcement ends. As L increases, the magnitude of u_r along the upper reinforcement surface tends to increase between $x = 1\,B$ and $3\,B$, in a manner similar to the upper shear stress distributions. Furthermore, the lower surface u_r values change from positive to negative slip, between $x = 1.8\,B$ and $4\,B$, for reinforcement lengths of $L \geq 1.96\,B$, which generates the inward clay shear stresses shown in Figure 9.3.

The profiles of the deformed membranes and the unreinforced interface, shown in Figure 9.6, illustrate that initial increases in the reinforcement length reduce the interface displacements appreciably, but that once the reinforcement reaches a length of $\approx 2\,B$ any continued increase in L has no significant influence.

9.3 General Conclusions

In practice a geosynthetic material at the interface of a two-layer soil system will often provide other functions, in addition to reinforcement, such as separation or filtration, which would clearly necessitate that the membrane covered the entire interface area. However, as a reinforcing layer exclusively, this parametric study shows that the width of the membrane needs only to be sufficiently wide enough to cover the area of subgrade influenced by both the normal and shear stresses generated at the interface. These fill and clay shear stresses exert a force on the membrane which produces the reinforcement tension, the magnitude of which is determined by the proportion of stresses that the membrane is able to pick-up.

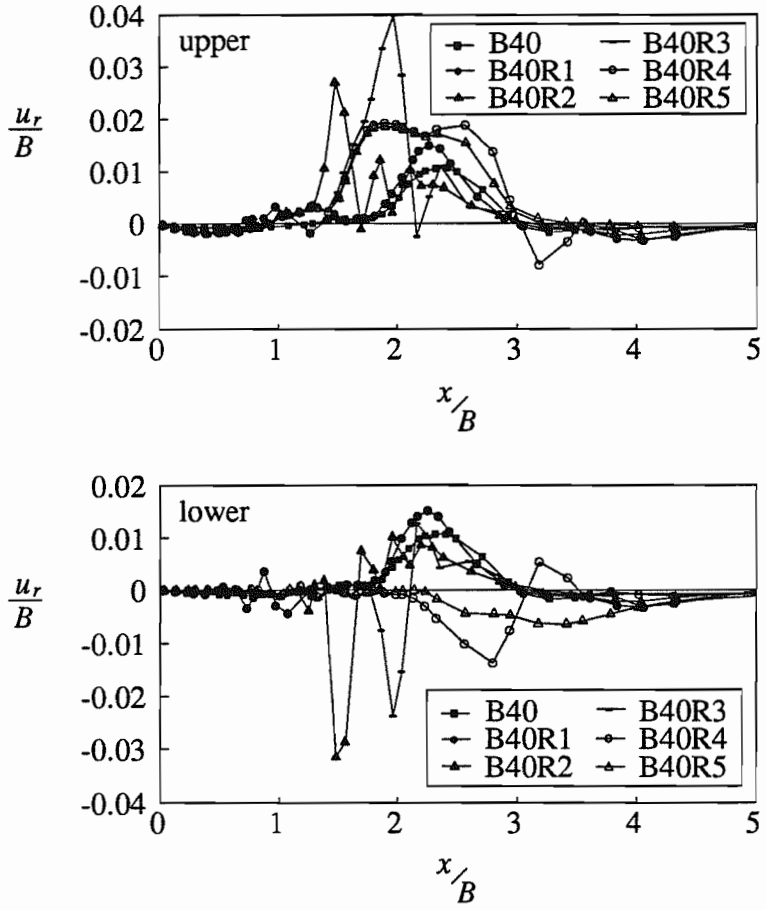

Figure 9.5: Relative Slip (u_r) along Interfaces

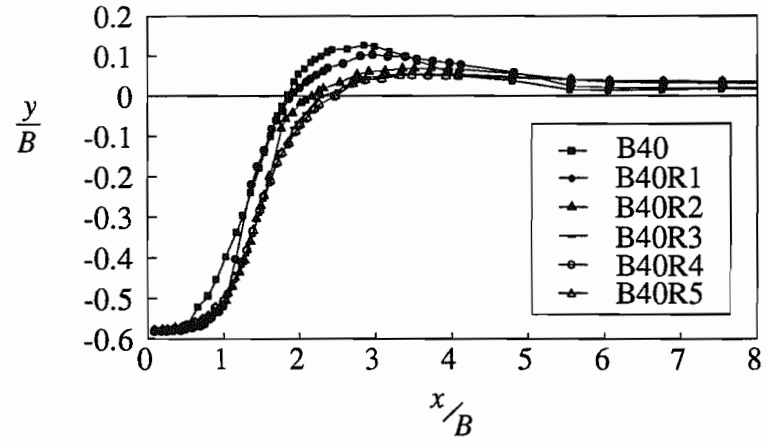

Figure 9.6: Final Deformed Shape of the Membranes

Therefore, with a reinforcement of width just greater than the imposed loaded area the tensioned membrane effect and the shear stress mechanism can operate adequately and provide a completely reinforced system. The significance of this is that the reinforcement

does not need to be anchored in any way prior to placing the fill, as was previously thought essential, to achieve the tensioned membrane effect. Thus, effective reinforcement can be achieved with only a minimum membrane width.

This result has further significance for the development of analytical models of membrane behaviour in two-layer soil systems. Many authors have attempted to develop simple analytical models to predict the membrane behaviour, but these, in general, have required fixities to be assumed at various points outside of the loaded area. In the development of any new models of behaviour it is clearly necessary to avoid the assumption of these spurious fixities.

CHAPTER 10:

INFLUENCE OF CLAY STRENGTH

10.1 Introduction

Reinforcement is often included in two-layer soil systems if the ground conditions are of poor quality with low, or seasonally very changeable soil strengths. The undrained shear strength of the subgrade soil, s_u, is therefore an important design parameter.

10.2 Parametric Study

For this study of how variations in the undrained shear strength of the clay effect the overall performance of a reinforced and unreinforced two-layer soil system, the parametric study is conducted for both plane strain and axisymmetric conditions, using meshes B and AXB (Figures 5.2 and 6.18) and the dimensions and properties of the soil and membrane given in Appendix 6A.

The plane strain shear strength values, s_u^{PS}, selected for this finite element parametric study are representative of the range of clay strengths that are typically encountered on the sites of two-layer soil systems; $10\,kPa$, $30\,kPa$ and $70\,kPa$. These undrained shear strengths are classified in the British Standard CP 2004 (1972) as "very soft", "soft" and "firm", respectively.

Although s_u^{PS} is varied in this parametric study, the clay shear modulus is kept constant at $G_c = 1600\,kPa$ and similarly the undrained Young's modulus, E_u, which is given by:-

$$E_u = 2\,G_c\,(1 + \nu_c) \tag{10.1}$$

where the Poisson's ratio is $\nu_c = 0.49$.

The von Mises constitutive model used in OXFEM (see Chapter 3) requires the triaxial compression value of shear strength, s_u^T, which is related to the plane strain value, in the limit that the elastic strain rates are negligible in comparison with the plastic strain rates, by the equation given in Burd (1986):-

$$s_u^{PS} = \frac{2}{\sqrt{3}} s_u^T \tag{10.2}$$

The plane strain value of the clay shear strength is used to categorise each finite element run for both the plane strain and axisymmetric analyses.

10.2.1 Load-Displacement Response

The footing pressure-displacement responses for each of the six plane strain and six axisymmetric, large displacement, finite element runs are illustrated in Figures 10.1 a) and b), and the results at a final displacement of $\delta = 0.6\,B\,;R$ are presented in Table 10.1, along with the comparative analytical predictions from the Houlsby *et al.* (1989) and Houlsby and Jewell (1990) methods. Note that the footing pressure, P , is normalised with respect to the clay shear modulus, G_c , rather than the clay shear strength as used in previous analyses.

The plane strain loading responses shown in Figure 10.1 a) for each value of s_u^{PS}, regardless of whether reinforced or unreinforced, possess an identical elastic stiffness. Similarly, the six axisymmetric loading responses shown in Figure 10.1 b) each have an identical elastic stiffness, which is approximately twice that of the plane strain. Clearly, the final footing pressures for the axisymmetric analyses are greater than the those for the corresponding plane strain analyses, Table 10.1.

The larger the prescribed value of s_u^{PS}, the greater the amount of footing displacement required before the plane strain and axisymmetric two-layer soil systems begin to yield plastically. At the same point of deviation from the linear elastic slope, the effect of the reinforcement becomes evident by maintaining a higher loading capacity compared to the equivalent unreinforced analysis. However, the proportional amount of loading

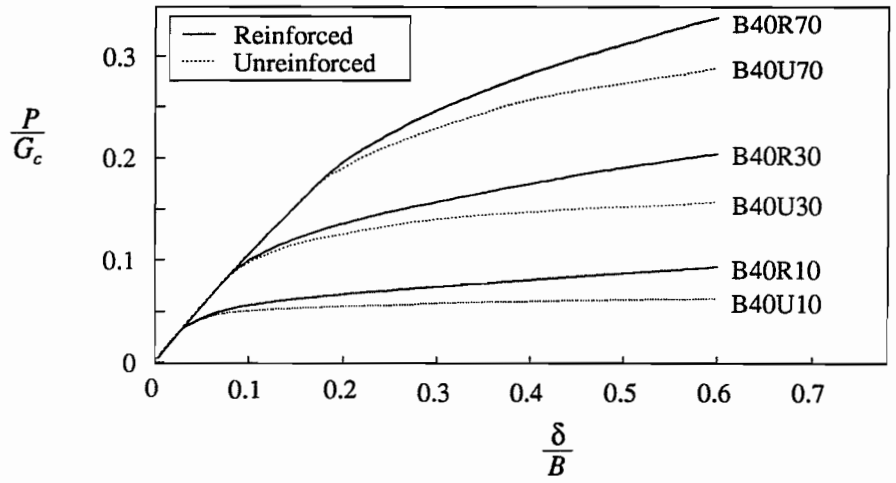

a) Plane Strain Analyses

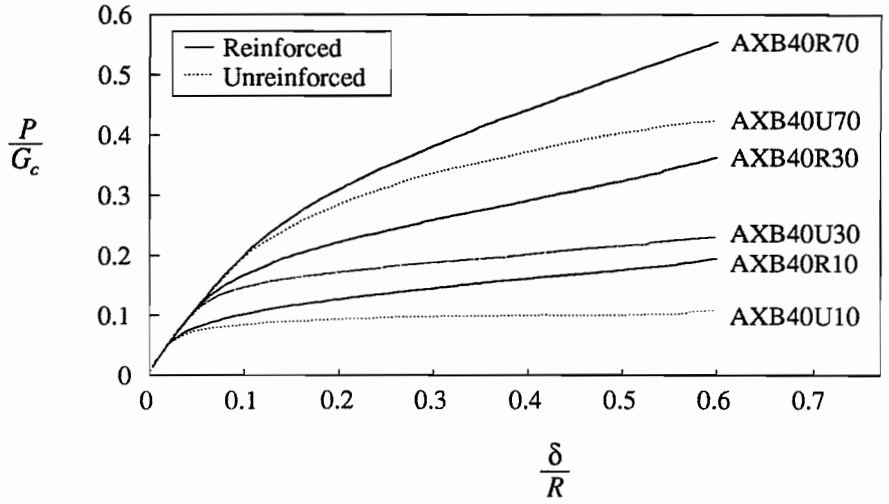

b) Axisymmetric Analyses

Figure 10.1: Pressure-Displacement Responses for Different Clay Strengths (s_u^{PS})

improvement obtained by including reinforcement reduces as the clay shear strength increases for both plane strain and axisymmetric conditions, i.e. for plane strain there is a 50% improvement for $s_u^{PS} = 10\ kPa$, 31% improvement for $s_u^{PS} = 30\ kPa$ and 18% improvement for $s_u^{PS} = 70\ kPa$ at a footing displacement of $0.6\,B$, while for axisymmetry there is a 79% improvement for $s_u^{PS} = 10\ kPa$, 52% improvement for $s_u^{PS} = 30\ kPa$ and 31% improvement for $s_u^{PS} = 70\ kPa$ at a footing displacement of $0.6\,R$.

				F.E.		Analytical		
	s_u^{PS}	δ_f	β	**Ref.**	P_f / G_c	**Ref.**	P_f / G_c	$F_r / (B\ G_c)$
	Plane Strain							
Reinf.	10	−14.8°	63.7°	B40R10	0.093	R10	0.110	0.034
	30	−10.3°	40.9°	B40R30	0.204	R30	0.197	0.062
	70	−5.9°	29.3°	B40R70	0.339	R70	0.376	0.105
Unreinf.	10	−9.5°	64.2°	B40U10	0.062	U10	0.086	-
	30	−8.0°	35.9°	B40U30	0.156	U30	0.123	-
	70	−5.6°	29.9°	B40U70	0.288	U70	0.256	-
	Axisymmetry							
Reinf.	10	−10.4°	39.3°	AXB40R10	0.195	AXR10	0.140	0.013
	30	−6.5°	27.2°	AXB40R30	0.363	AXR30	0.279	0.047
	70	−3.9°	22.1°	AXB40R70	0.554	AXR70	0.551	0.109
Unreinf.	10	−13.0°	40.0°	AXB40U10	0.109	AXU10	0.101	-
	30	−10.5°	29.8°	AXB40U30	0.239	AXU30	0.146	-
	70	−8.1°	24.3°	AXB40U70	0.423	AXU70	0.238	-

Table 10.1: Run References for the Plane Strain and Axisymmetric Finite Element and Analytical Results Shown in Figures 10.1

From Table 10.1 it is clear that as s_u^{PS} increases the outward acting angle of friction on the footing base (δ_f) decreases for both the plane strain and axisymmetric analyses, although the actual footing frictional force ($P_f B \tan\delta_f$, or $P_f R \tan\delta_f$) increases.

Similarly the load spread angle (β) also decreases with increasing clay shear strength, as seen clearly in the normal and shear stress distributions in Figures 10.2 and 10.3. The

large values of β for the very soft clay analyses are comparable to those found by Milligan *et al.* (1989). By comparing the results of the large-scale experimental axisymmetric tests of Fannin (1986) and the Houlsby and Jewell (1990) analytical method, Milligan *et al.* (1989) found that an appropriate value of β was in the range 45° - 50°, for the case of a strong fill ($\phi = 45°$) over weak clay ($s_u = 8\ kPa$). The smaller range of β values for the axisymmetric analyses, compared to plane strain, is due to the more rapid reduction of the vertical stress within the fill than occurs in plane strain conditions.

The reinforced ultimate footing loads predicted by the Houlsby *et al.* (1989) and Houlsby and Jewell (1990) methods for the plane strain and axisymmetric cases, Table 10.1, are mostly reasonable approximations to the finite element results. For the unreinforced cases, however, the analytical solutions are generally less comparable to the finite element results, because of the incorrect assumption that the shear stresses are consistently outward acting at the fill base, see Figures 10.2 and 10.3.

10.2.2 Normal and Shear Stress Distributions

All the normal (σ) and shear (τ) stress distributions shown in Figures 10.2, for plane strain, and 10.3, for axisymmetry, are normalised with respect to the particular value of the plane strain shear strength prescribed for that individual run.

By increasing the shear strength from $s_u^{PS} = 10\ kPa$ to $70\ kPa$ there is a noticeable reduction in the non-dimensionalised normal stresses (although an increase in the absolute values), in both the reinforced and unreinforced plane strain and axisymmetric analyses. This is partly because the magnitude of the inward shear stresses acting on the clay, just outside the load spread area, reduce from $\tau \approx -1\ s_u^{PS}$ (slightly greater than the shear strength of the clay due to discretization errors) to about zero as the clay shear strength is increased and consequently the bearing capacity factor of the clay decreases. For plane strain conditions this reduction in N_c is from the absolute maximum of $(1 + 3\pi/2)$ to $(2 + \pi)$ (i.e. from Mode 2 to Mode 1 in Figure 6.16), whereas for axisymmetric conditions the approximate reduction in N_c is from $\approx 1.11 \times 6.3$ to 6.3 (see Section 6.4.2). Thus, for the $s_u^{PS} = 70\ kPa$ analysis the lower normal stresses at the footing centre-line approximately reduce to the plasticity solution of $(\pi + 2)\, s_u^{PS} + \gamma_f D_f \approx 5.2\, s_u^{PS}$ in plane strain and

$6.3\,(\sqrt{3}/2)\,s_u^{PS} + \gamma_f D_f \approx 5.5\,s_u^{PS}$ in axisymmetry. Additionally, an increase in shear strength also decreases the load spread angle (see Table 10.1), which is evident in all of the upper and lower normal stress distributions illustrated in Figures 10.2 and 10.3. This same effect was experimentally observed by Love (1984), (as shown in Tables 7.3 and 7.4), and is also predicted by the theoretical relationship derived from the Meyerhof (1974) analysis, given as equation (7.6).

The difference between the upper and lower reinforced normal stress profiles gives a measure of the tensioned membrane effect, which clearly has a diminishing influence as the clay strength increases in both the plane strain and axisymmetric analyses. This result is also apparent from the smaller percentages of improvement obtained in the pressure-displacement responses as s_u^{PS} increases, Figure 10.1. By comparing the plane strain and axisymmetric upper normal stress distributions it is clear that the tensioned membrane effect is greater in axisymmetric conditions for any particular value of s_u^{PS}.

The magnitudes of the plane strain and axisymmetric non-dimensionalised shear stresses on the upper and lower reinforcement surface decrease (but increase in absolute value) for increasing s_u^{PS}, and effect a significantly reduced area along the reinforced interface due to the smaller load spread angle. The shear stress mechanism of the reinforcement is evident by comparing the consistently outward acting shear stresses on the lower reinforcement surface to the alternating inward/outward acting shear stresses at the unreinforced interface. The exceptionally high peak inward acting shear stresses for runs B40R10 and AXB40R10 are spuriously caused by discretization errors, as explained in Section 5.4.5. The peak outward shear stresses in the unreinforced analyses reach a critical value of $1\,s_u^{PS}$ at around $x = 1.5\,B \rightarrow 2\,B$ and $r = 1.5\,R \rightarrow 1.8\,R$.

Plane Strain

NORMAL STRESS **SHEAR STRESS**

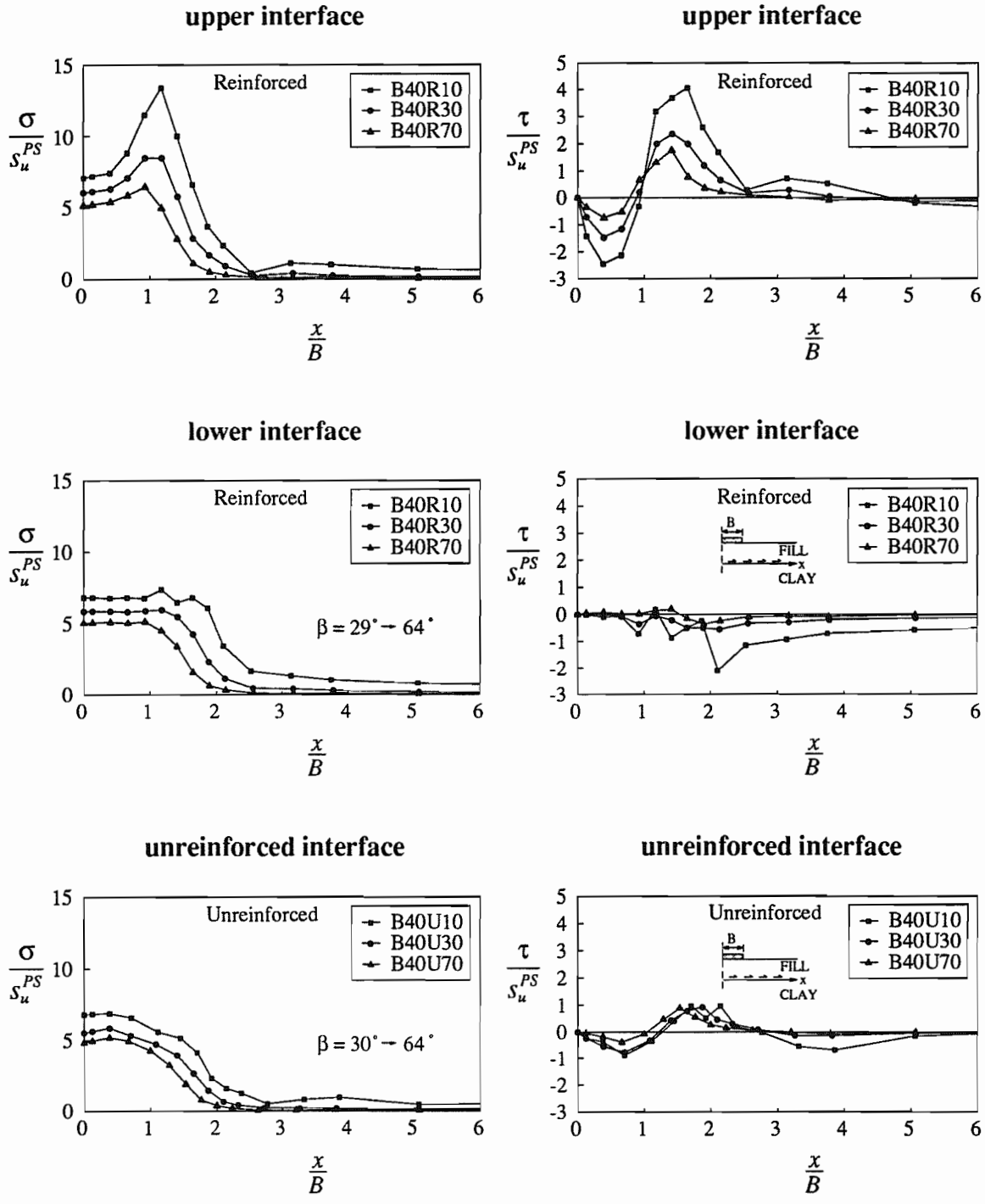

Figure 10.2: Normal (σ / s_u^{PS}) and Shear (τ / s_u^{PS}) Stresses along Interface for Varying Clay Strengths (s_u^{PS}) in Plane Strain, (at $\delta = 0.6\,B$)

Axisymmetry

NORMAL STRESS **SHEAR STRESS**

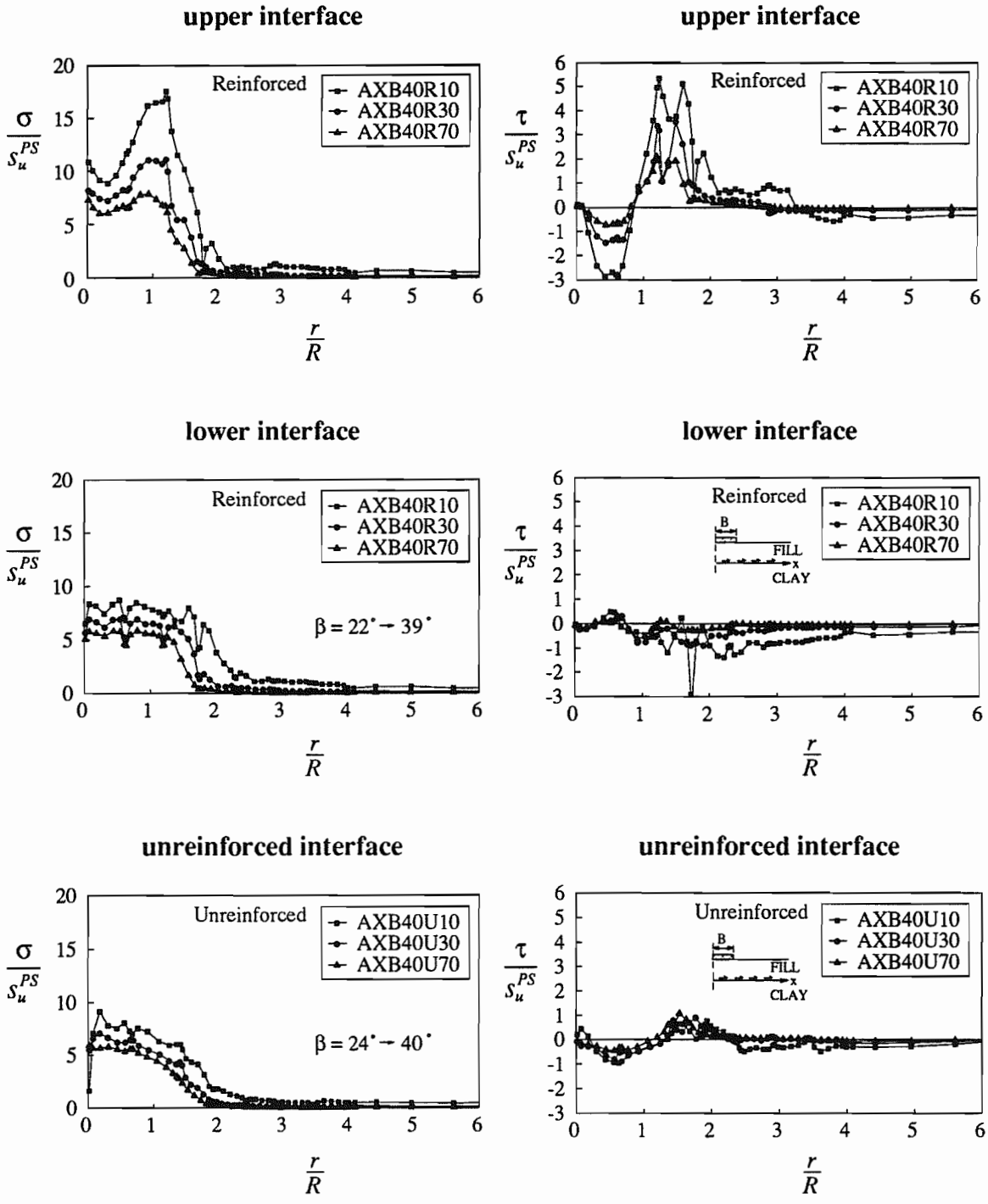

Figure 10.3: Normal (σ / s_u^{PS}) and Shear (τ / s_u^{PS}) Stresses along Interface for Varying Clay Strengths (s_u^{PS}) in Axisymmetry, (at $\delta = 0.6\,R$)

10.2.3 Reinforcement Tension Distribution

The reinforcement tensions (longitudinal, F_r , in plane strain and tangential, F_{tang} , and circumferential, F_{circ} , in axisymmetry) developed at the final footing displacement of $\delta = 0.6\,B; R$ are normalised in Figure 10.4 by the product of B , or R , and the clay shear modulus, G_c , rather than $B\ s_u^{PS}$ as used in the previous parametric studies.

The peak tensions, reached at about $x = 1\,B$ in plane strain and $r = 0.7\,R$ in axisymmetry, increase with higher clay strengths because of the larger absolute shear forces acting on the membrane. However, the rate of reduction of the longitudinal and tangential reinforcement tensions along the membrane is quicker, in terms of distance, for higher values of s_u^{PS} , because of the smaller load spread area in which the upper and lower shear stresses are concentrated, see Figures 10.2 and 10.3. The peak circumferential tensions are slightly lower than the peak tangential tensions, for any particular run, but do not reduce to zero as quickly and extend for a greater horizontal distance.

The analytical predictions of the tensions, given in Table 10.1, are poor approximations of the peak finite element values. For $s_u^{PS} = 10\ kPa$ and $30\ kPa$ the analytical values of the tensions are too low and for $s_u^{PS} = 70\ kPa$ they are too high, for plane strain and axisymmetry.

10.2.4 Slip and Deformation along Interfaces

The relative slip, u_r , along the unreinforced and the upper and lower reinforced surfaces is illustrated in Figure 10.5, for plane strain and axisymmetry. Significant slip continues for greater horizontal distances in the plane strain analyses than exists in axisymmetry.

As the clay strength increases, the magnitude of the slip at the unreinforced and upper reinforced surfaces increases also, in both plane strain and axisymmetry, as do the absolute shear stresses shown in Figures 10.2 and 10.3. Along the lower reinforced surface, however, the magnitude of the slip actually decreases as s_u^{PS} is increased, in contrast to the magnitude of the lower absolute shear stresses. It is noteworthy that for the unreinforced very soft clay analyses ($s_u^{PS} = 10\ kPa$), the general trend of the fill slipping out over the clay, diminishes to approximately zero in axisymmetry, while for plane strain the slip actually reverses so that the clay tends to slide out from under the fill.

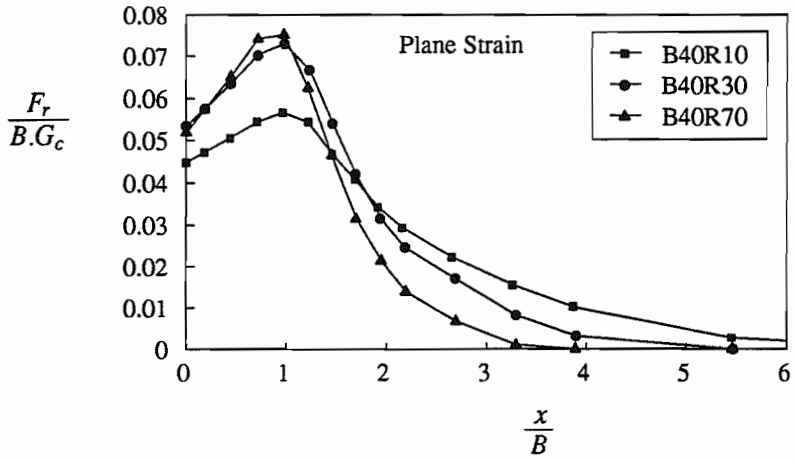

Plane Strain (longitudinal)

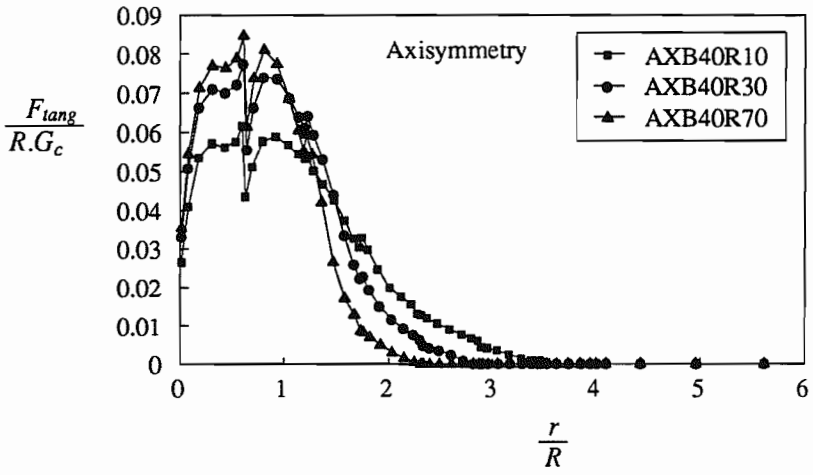

Axisymmetry (tangential)

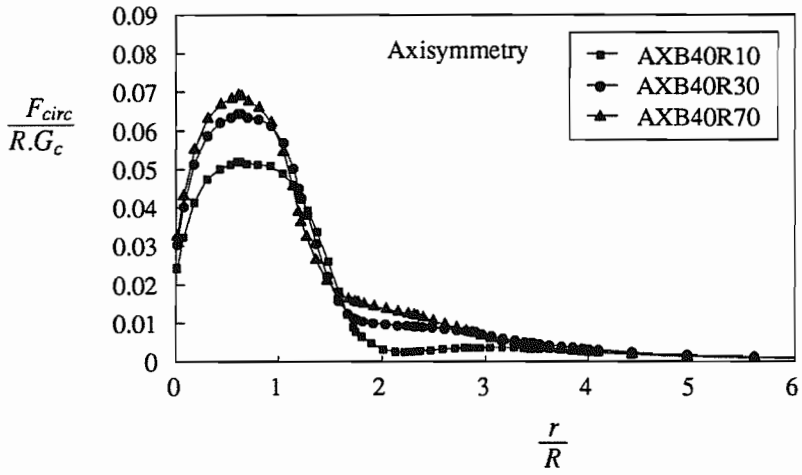

Axisymmetry (circumferential)

Figure 10.4: Reinforcement Tensions for Different Clay Strengths, (at $\delta = 0.6\,B\,;\,R$)

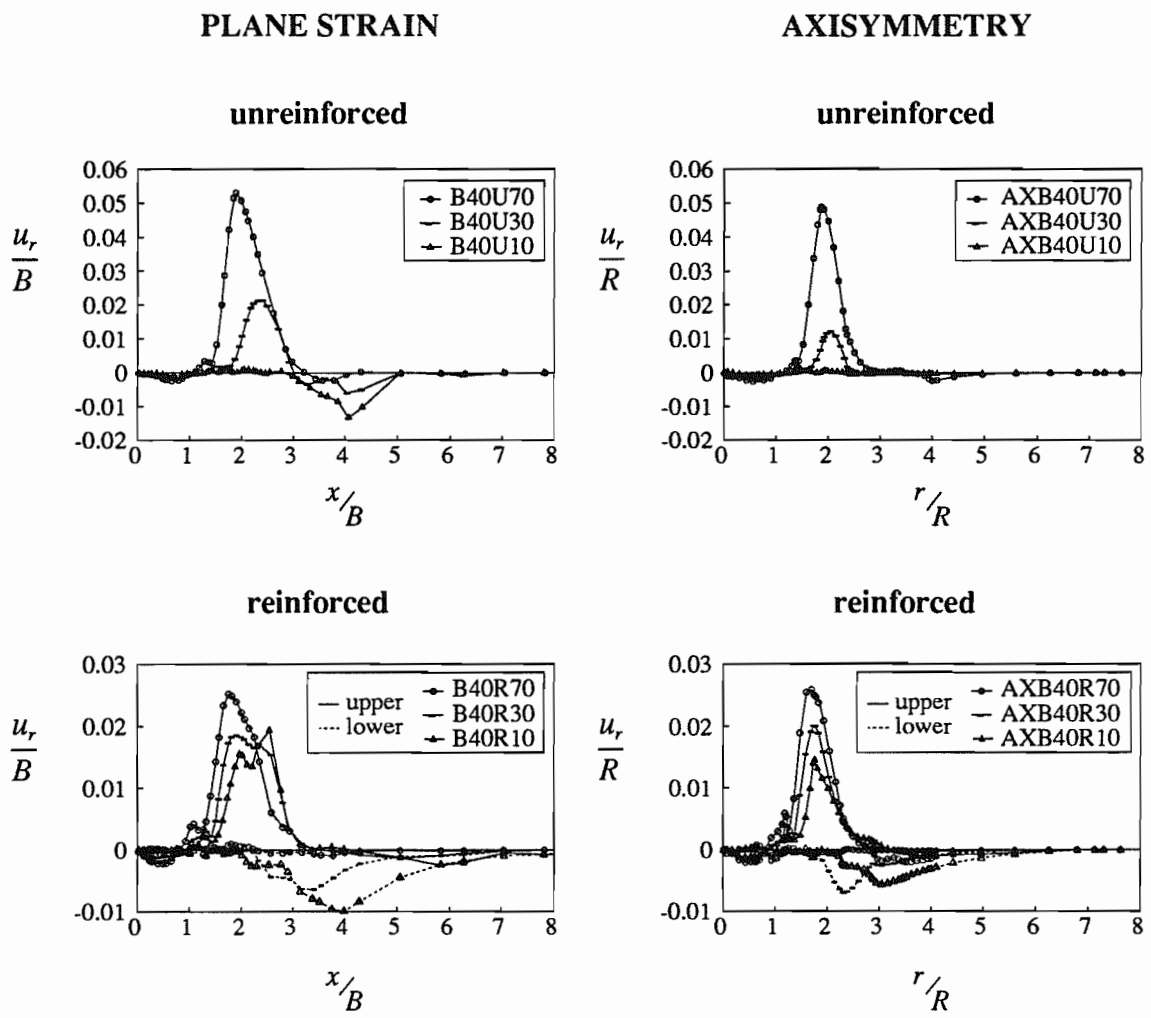

Figure 10.5: Relative Slip (U_r) along the Interfaces

The shape of the final deformed interfaces, shown in Figure 10.6, vary according to the clay strength, with smaller vertical displacements for the stiffer clay. The reinforcement tends to reduce the interface deformations, although for plane strain conditions the magnitude of the vertical displacements, beyond $x = 2B$, is greater generally than those for axisymmetry beyond $r = 2R$.

10.3 General Conclusions

There is a dramatic effect upon the mechanics of a plane strain and an axisymmetric two-layer soil system for variations in the undrained shear strength of the clay subgrade. Increasing the clay shear strength obviously necessitates an increased footing pressure to obtain the

same vertical displacement, but simultaneously this reduces the proportional contribution of the tensioned membrane mechanism to the overall reinforcement of the system. Additionally, the load spread angle also reduces with increasing clay strength, so that the area along the interface in which the normal and shear stresses act, diminishes significantly.

The Houlsby *et al.* (1989) and Houlsby and Jewell (1990) design methods give reasonable indications of the value of the ultimate footing load on a reinforced two-layer soil system for a variety of clay strengths, but less accurate estimates for the unreinforced system. The predicted reinforcement tensions are also inaccurate, because of the simplified approach used in the limit equilibrium methods to estimate the complex arrangement of inward and outward acting shear forces applied to the membrane.

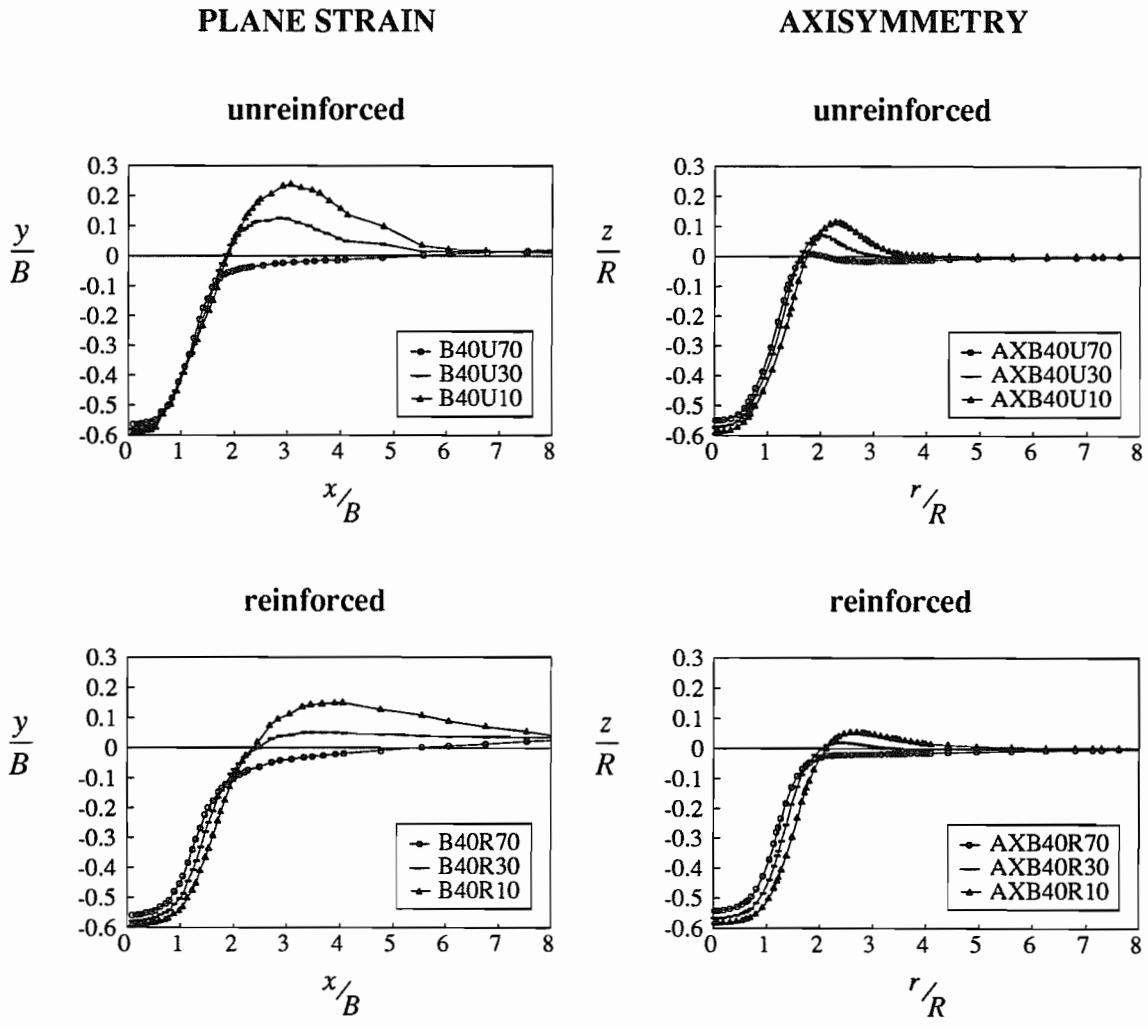

Figure 10.6: Final Deformed Shape of the Interfaces

CHAPTER 11:

ANALYSIS OF LOW FRICTION MEMBRANES IN GRANULAR BASES

11.1 Introduction

The application of the newly developed axisymmetric interface element (detailed in Chapter 5) to the analysis of the use of membranes in granular base foundations is described in this chapter. The particular application considered is for the comparatively new and relatively unresearched problem of low friction polymeric membranes incorporated within the compacted fill base of oil storage tanks, to provide secondary containment against oil leakage from damaged, or corroded tanks. The purpose of this study is to investigate numerically how the presence and configuration of a low friction membrane influences both the surface displacements and the soil deformations at the tank edge, for various values of plane strain fill friction angle (ϕ_{PS}) and shear modulus (G_f).

Extensive research has been carried out at the University of Oxford on the use of low friction membranes in oil tank bases and the problem of predicting the amount of edge displacement developed by filling the tank, i.e. 'edge cutting'. This is important because the rut created by edge cutting can become a moisture trap, leading to accelerated tank corrosion. This chapter gives a qualitative synopsis of that research, which is fully documented in Burd *et al.* (1993). However, due to contractual agreements on confidentiality, the complete set of data and detailed analyses have been omitted.

11.2 Design of Oil Storage Tanks

Large steel oil storage tanks are flexible structures and transmit the weight of their liquid contents to their foundation as a uniform distributed load. Designs for such tanks have to accurately predict and allow for deformations of the structure and the underlying ground, which clearly requires a rigorous site investigation and precise design specifications. Unfortunately this has not always been achieved and full-scale failures of oil tanks have not been uncommon in the past, e.g. Nixon (1949) and Brown and Paterson (1964).

If the subgrade soil is strong enough to support the weight of the tank, the simplest form of foundation consists of a pad of granular material, usually less than 1 *m* thick, placed directly on the exposed subgrade, Figure 11.1. The pad is generally made thicker at the centre than at the edges (typically a 1:120 slope) since central settlements are expected to be greater than the edge settlements. The dimensions of a typical oil storage tank, as assumed for this study, and the base edge details are shown in Figure 11.1.

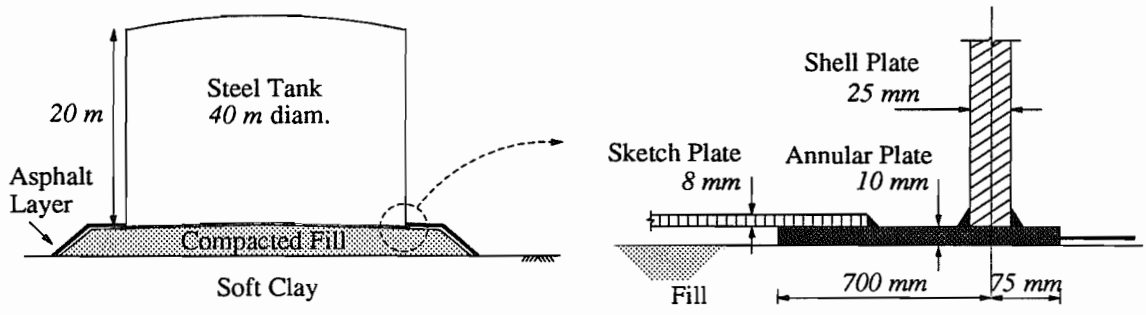

Figure 11.1: Simple Oil Storage Tank Foundation
(Schematic Diagram)

The risk of ground pollution and the structural dangers of reduced foundation stability, caused by any amount of oil leakage, have become of increasing concern recently. This has led to the use of impermeable membranes within the fill layer for leak detection and containment purposes.

The recommended Standard for welded steel oil storage tanks (A.P.I. 650) illustrates typical designs for the installation of membranes as undertank leak detection systems, for example Figure 11.2.

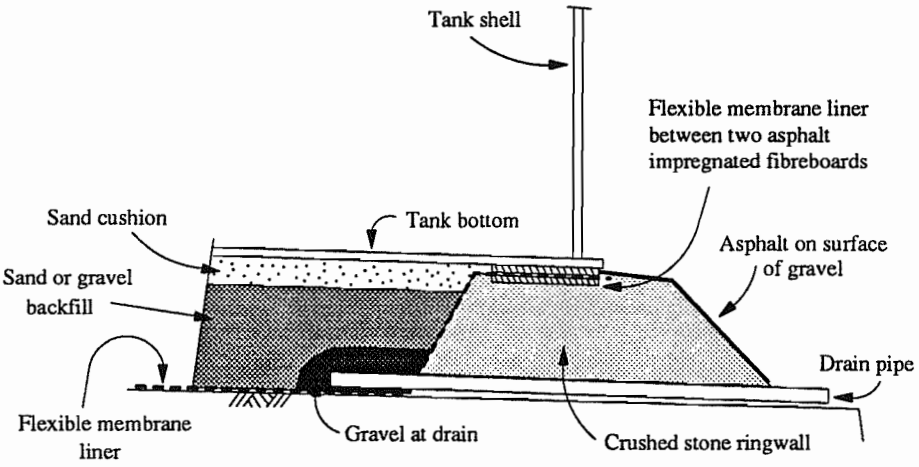

Figure 11.2: Typical Tank Perimeter Design
(After A.P.I. 650 Appendix I)

It is possible, however, that the inclusion of a low friction membrane may introduce a plane of weakness, which could lead to unacceptably increased settlements under the tank. Additionally, the presence of a membrane beneath the tank edge may exacerbate the problem of soil heave around the perimeter of the tank caused by edge cutting.

11.3 Idealization of the Problem

The problem is idealized in order to conduct a large displacement axisymmetric finite element investigation. Since it is the local edge deformations within the fill that are important in this study, it is not necessary to include the layer of subgrade soil in the analysis. This means that the fill deformations are computed correctly, but that the general elastic settlements, predicted beneath the tank as a whole, would be inexact with this approach. Additionally, the finite element mesh only needs to extend a sufficient distance, either side of the edge, so that any mesh boundary effects are removed (see Figure 11.5).

The fill is represented as an elastic perfectly-frictional material, modelled by the Matsuoka yield function (discussed in chapter 3), and the steel tank is modelled using a linearly elastic perfectly-plastic model (based on the von Mises yield criterion). The soil and tank are both modelled using fifteen-noded axisymmetric triangular continuum elements (illustrated in Figure 3.1) with a sixteen-point Gauss quadrature. Some initial analyses employed a thirteen-point Gauss quadrature, but this proved to be numerically unstable. The membrane is modelled using the ten-noded axisymmetric frictional interface element with a seven-point Gauss rule, as described in Chapter 5.

The shell plate of the tank is modelled by a 'stub wall' of thickness 0.025 m and height 1.5 m, rather than the complete 20 m height which would require an excessively large number of elements. It is thought, however, that the important features of the interaction between the tank and the foundation are modelled adequately by this approach. A horizontal constraint is applied to the inside bottom edge of the annular plate in order to simulate the presence of the sketch plate. The simplified tank base details, used in the finite element investigation, are shown in Figure 11.3.

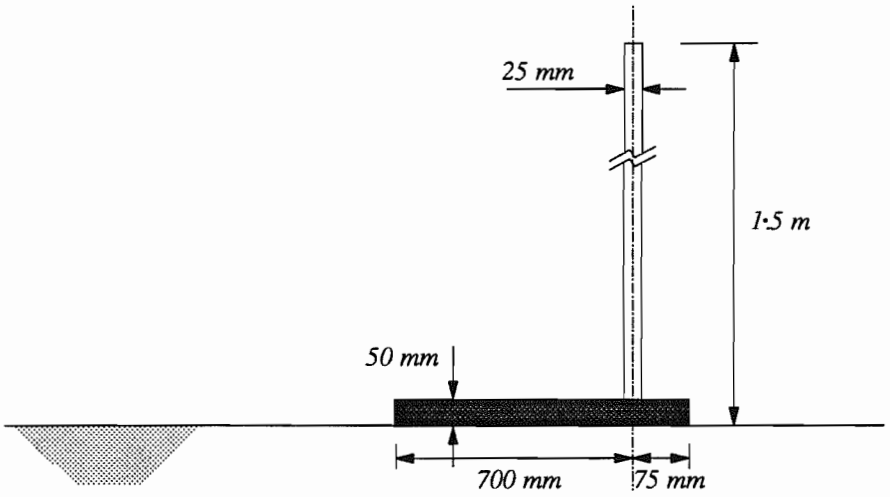

Figure 11.3: Idealized Model for Tank Edge

(After Burd *et al.* (1993))

Due to the large range of material stiffnesses considered in this problem (i.e. the relatively high steel stiffness compared to the low soil stiffness), ill-conditioning of the finite element global stiffness matrix might be expected to occur. Such ill-conditioning can be moderated by reducing, if possible, the high steel stiffness. Therefore, the prescribed stiffness of the annular base plate is reduced by a factor of 125 and the thickness is increased by a factor of 5, to preserve the important bending stiffness, (as shown in Figure 11.3). Similar modifications of the tank wall properties, however, are considered inappropriate since both the bending and axial stiffnesses of the wall have an important effect on its structural behaviour.

The finite element calculations are all load controlled, with the loads taken to be the values typical of an oil tank. The stresses due to the fill self weight are assigned initially, followed by two separate loading stages. The first stage applies increments of nodal forces equivalent to the combined self weights of the tank (41 kN/m) and the oil (10 kN/m^3). The tank self weight is applied at the base of the wall. The original intention was not to apply these loads simultaneously, but as two separate stages. However, this proved difficult because of the numerical instability caused by the eccentric loading of the annular plate under the tank self weight only, whereas by combining it with the oil weight the annular plate is loaded more evenly. The second stage consists of the further application of load, at the base of the wall, corresponding to both the wind (15 kN/m) and the roof surcharge (5 kN/m) loading.

Hydrostatic loads are calculated from the hydrostatic stresses for increments of the oil depth H, shown in Figure 11.4, and applied at the relevant nodes. This calculation is based on the standard virtual work approach and the vector of the nodal forces, $\underset{\sim}{P}$, is given by:-

$$\underset{\sim}{P} = 2\pi \int_E [N]^T w\, r\, ds \tag{11.1}$$

where the shape function matrix, $[N]$, is given by the equations (4.64) to (4.69) and w is the hydrostatic pressure. The integration is performed over the element length, using a

seven-point Gaussian quadrature scheme. The oil depth is increased to a maximum of $20\ m$. For every increment of oil level inside the tank, one of three loading cases exists for each of the elements along the base and inside wall of the tank;

1) All the nodes are above the oil surface:

   No nodal loads are applied.

2) The oil surface intersects the element:

   Only relevant for vertical elements, where the submerged nodes are loaded linearly with height and those above the oil level are allocated zero nodal force.

3) All the nodes are below the oil surface:

   For horizontal elements the pressure is constant,

   For vertical elements the pressure over the element is linear with height.

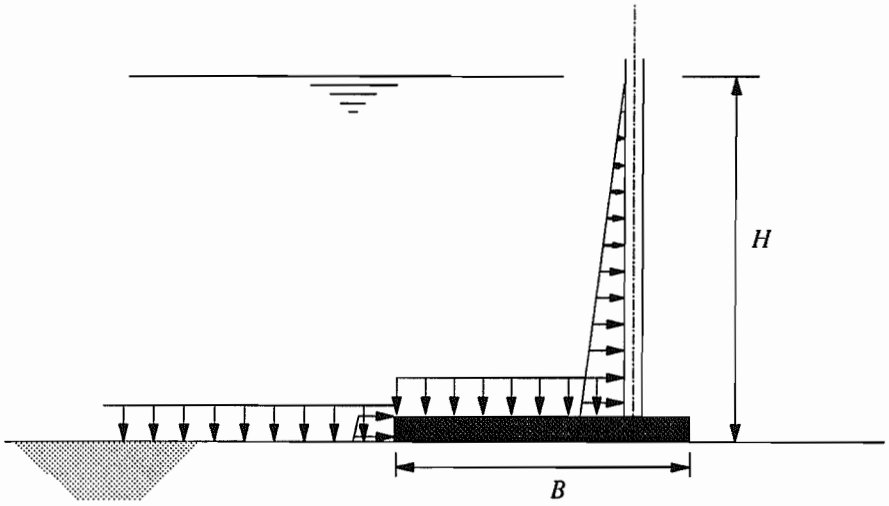

Figure 11.4: Application of Oil Loading

(After Burd *et al.* (1993))

This study considers the oil tank foundation initially without a membrane (Mesh I, Figure 11.5) and then three cases for different configurations of the membrane position within the fill. Firstly, with the membrane horizontal across the entire mesh width, at a depth of $d = B / 3$, where B is the width of the annular plate equal to $775\ mm$ (Mesh II, Figure 11.5). Secondly, for a similar arrangement, but with $d = 2B / 3$ (Mesh III, Figure 11.6) and finally with the membrane again horizontal at a depth of $d = 2B / 3$ beneath the tank, but inclined at 50° under the annular plate and terminating at the outside edge of the

annular plate (Mesh IV, Figure 11.7). The 50° inclination, from the horizontal, of the membrane in mesh IV is considered to represent the worst recommended design case (Figure 11.2). The end detailing of the membrane in Mesh IV requires that the last upper node of the interface element (i.e. node 7 in Figure 5.16) is common with the annular plate edge and that the last lower interface node (i.e. node 2 in Figure 5.16) is common with the underlying soil.

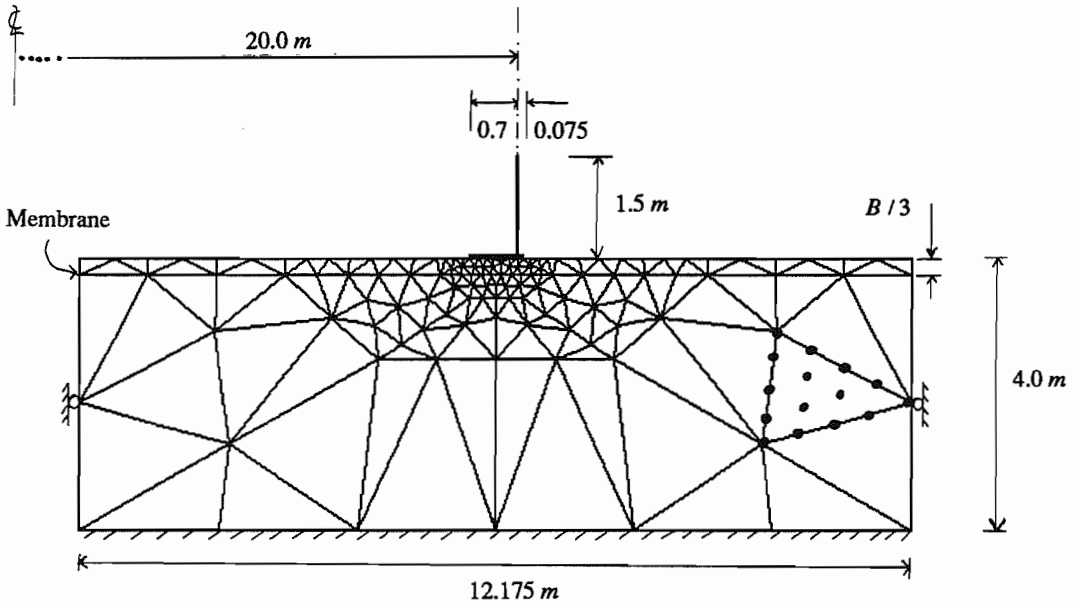

Figure 11.5: Mesh I - No Membrane
(Mesh II - Membrane at level indicated)
(After Burd *et al.* (1993))

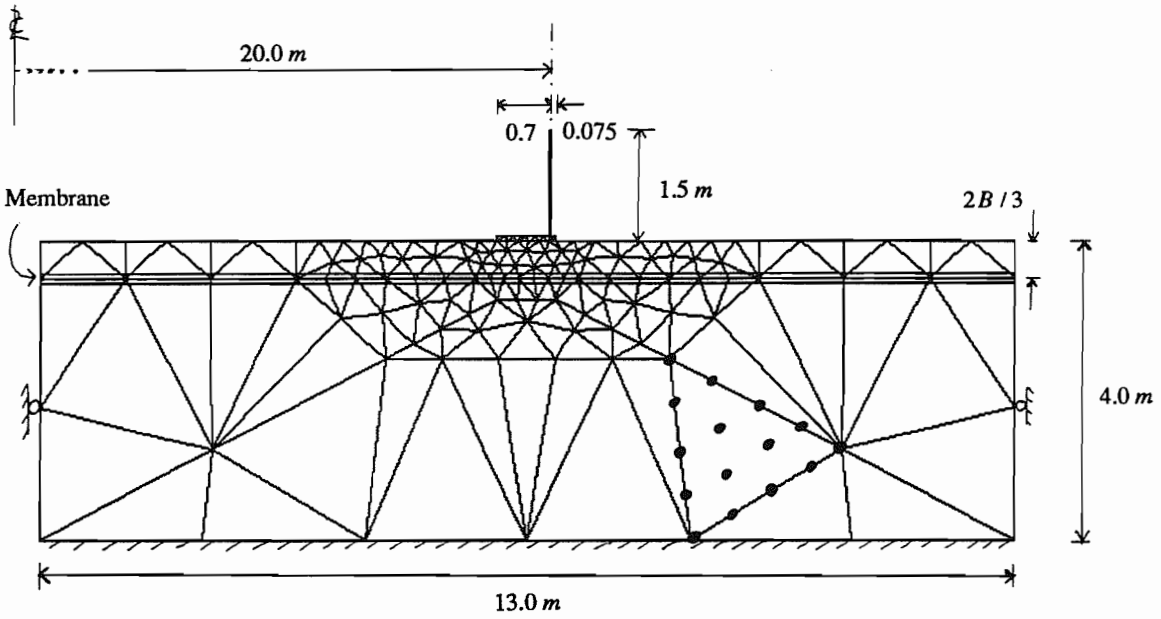

Figure 11.6: Mesh III

(After Burd *et al.* (1993))

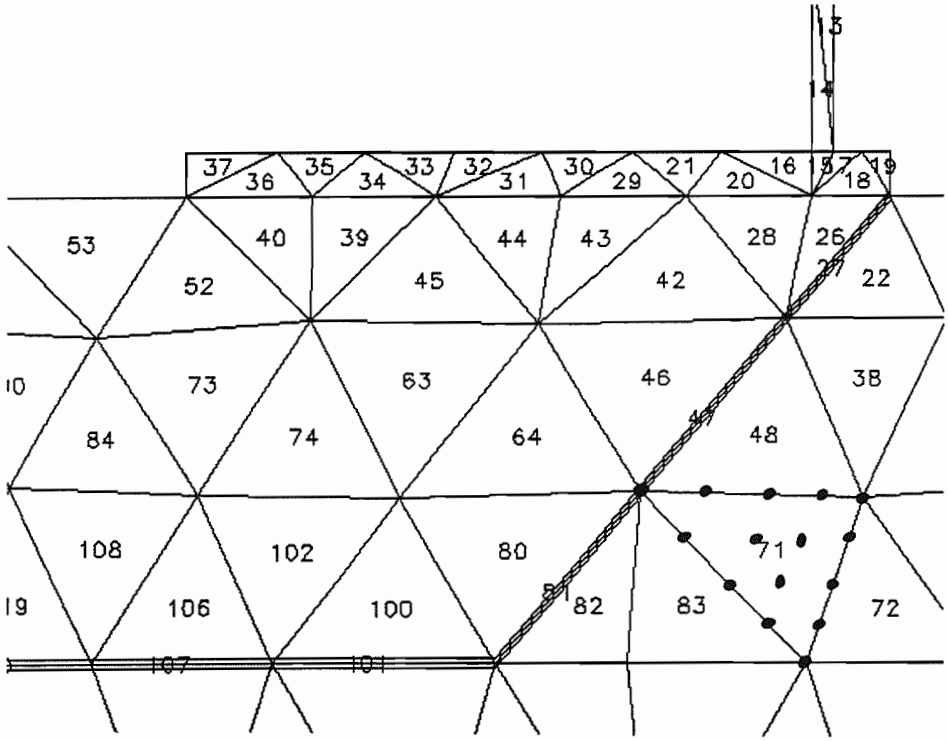

Figure 11.7: Detail of Mesh IV with Element Numbers

(After Burd *et al.* (1993))

11.4 Specification of Material Properties

A series of finite element calculations is described, for each of the different meshes, with various prescribed values of plane strain fill friction angle (ϕ_{PS}) and shear modulus (G_f).

Three different values of ϕ_{PS} are chosen (32°, 40° and 48°) which represent a material with a critical state friction angle ϕ_{cv} of 32° compacted to different densities. The Poisson's ratio of the fill, ν_f, is set to 0.2 and the value of the plane strain dilation angle, ψ_{PS}, is assumed to be given by the empirical relationship proposed by Bolton (1986):-

$$\phi_{PS} = \phi_{cv} + 0.8\,\psi_{PS} \tag{11.2}$$

The variations in the plane strain dilation angle are believed to have only a minor influence on the behaviour of the fill for this type of loading situation, as suggested in Section 7.2, but nevertheless are considered here for the sake of completeness.

Two values of soil shear modulus are selected, $G_f = 3\,000\ kPa$ as a lower bound stiffness and $G_f = 12\,000\ kPa$ as an upper bound value. The finite element calculations are listed in Table 11.1, referenced by the relevant mesh used (i.e. Mesh I, II, III, or IV), along with the corresponding final vertical displacements, calculated at the outside edge of the annular plate for each run.

For runs II, III and IV the membrane is assumed to have an angle of friction ϕ_i of 10°, which is a credible lower bound value for smooth membranes, and zero dilation angle. It is important to chose appropriate values for the elastic shear and normal stiffnesses (k_s and k_n respectively), because values that are too high will result in ill-conditioning and too low will lead to significant additional shear and normal displacements. The stiffnesses are derived from the equations:-

$$k_s = \frac{G_f}{L_c} \tag{11.3}$$

$$k_n = \frac{E}{L_c} = \frac{2\,G_f\,(1+\nu_f)}{L_c} \tag{11.4}$$

where the characteristic length L_c corresponds to a nominal thickness of the interface. It is assumed that L_c = 0.1 m for the calculations using Meshes II and III, and 0.05 m for the Mesh IV runs. This increased stiffness for the sloping membrane runs was considered appropriate in order to assure numerical stability.

Runs Referenced by Mesh No.		
ϕ_{PS}	$G_f = 3\,000\ kPa$	$G_f = 12\,000\ kPa$
32°	I; II; III; IV 1	I; II; III; IV 2
40°	I; - - IV 3	I; - - IV 4
48°	I; II; III; IV 5	I; II; III; IV 6
Corresponding Vertical Displacements of Annular Plate Perimeter (*mm*)		
ϕ_{PS}	$G_f = 3\,000\ kPa$	$G_f = 12\,000\ kPa$
32°	162; 164; 183; 190	45; 51; 46; 57
40°	112; - - 111	32; - - 44
48°	89; 94; 93; 94	24; 26; 25; 27

Table 11.1: Finite Element Referencing and Calculated Edge Displacements

In all the analyses the bulk unit weight of the fill (γ_f) is taken to be 18 kN/m^3. The initial vertical stresses (σ_v) are computed directly from the self weight and the horizontal stresses for runs I, II and III, are calculated as $K_0\,\sigma_v$, using a specified value of the earth pressure coefficient, K_0, given by the Jaky expression:-

$$K_0 = 1 - \sin\phi_{PS} \tag{11.5}$$

For runs IV this value of K_0 is inappropriate, since the mobilised friction angle on the sloping portion of the membrane would exceed 10°. It is possible to show that the value of

K_0, which would just cause failure, is given by:-

$$K_0 = \frac{1 - \sin\phi_i}{1 + \sin\phi_i} \approx 0.7041 \tag{11.6}$$

Therefore, a value of $K_0 = 0.71$ is used for the Mesh IV runs.

11.5 Discussion of Results

The results presented in Table 11.1 show that as the fill strength increases all of the predicted edge vertical displacements reduce significantly, and that increasing the shear modulus from 3 000 kPa to 12 000 kPa has the effect of decreasing the displacements by a factor of approximately 3.5.

Incorporating a low frictional membrane into the fill, clearly increases the edge displacements of the annular plate, compared to the case where the membrane is absent (Mesh I). For the configurations of the membrane that extend horizontally beyond the tank perimeter (Meshes II and III), the additional vertical displacements are all relatively small, with no obvious indication as to which of the membrane depths is most adverse. The sloping membrane case (Mesh IV), however, produces the largest edge displacements (except for $\phi_{PS} = 40°$ and $G_f = 3\,000\ kPa$, run IV3, which is thought to be spuriously low).

The edge cutting of the annular plate into the fill and the exact relative distortions within the soil are seen clearly in the final deformed meshes, two of which are illustrated in Figures 11.8 and 11.9. Small rotations of the loaded annular plate are discernible, particularly for run IV1 (Figure 11.9). Inside of the annular plate the vertical settlements are approximately uniform and these diminish with depth, while the horizontal movements are comparatively insignificant. The relative soil slip between the upper and lower membrane surfaces is visible from these deformed meshes (investigated in more detail later) and, in Figure 11.9 particularly, the interpenetration of the continuum elements across the slip plane is also perceptible. This small overlap of the elements is due to the finite normal stiffness (k_n), which is assigned to the interface elements to avoid numerical instability, and is approximately equal to σ_v / k_n.

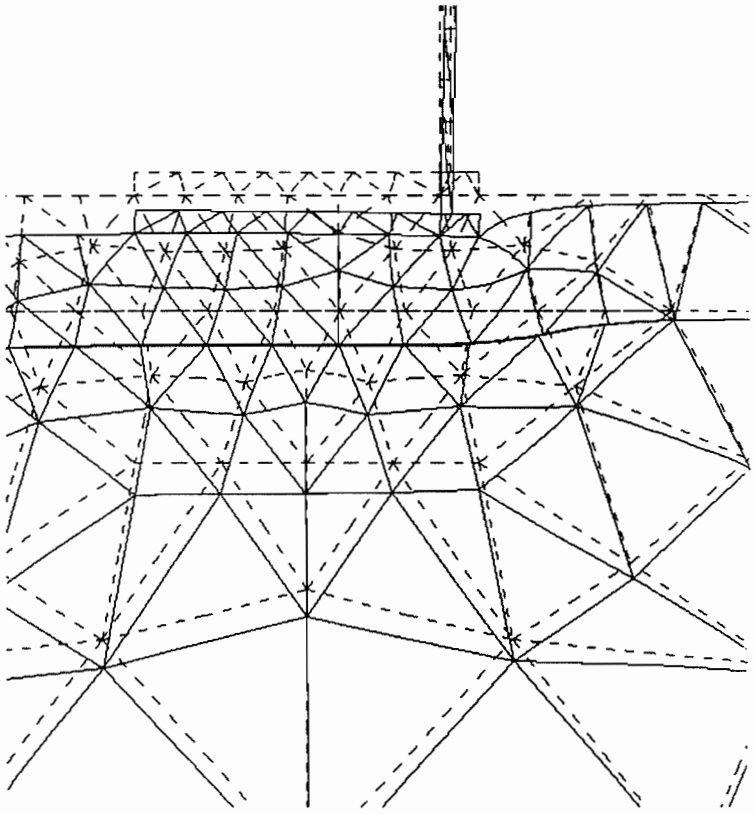

Figure 11.8: Undeformed and Corresponding Deformed Mesh for run II5 (After Burd *et al.* (1993))

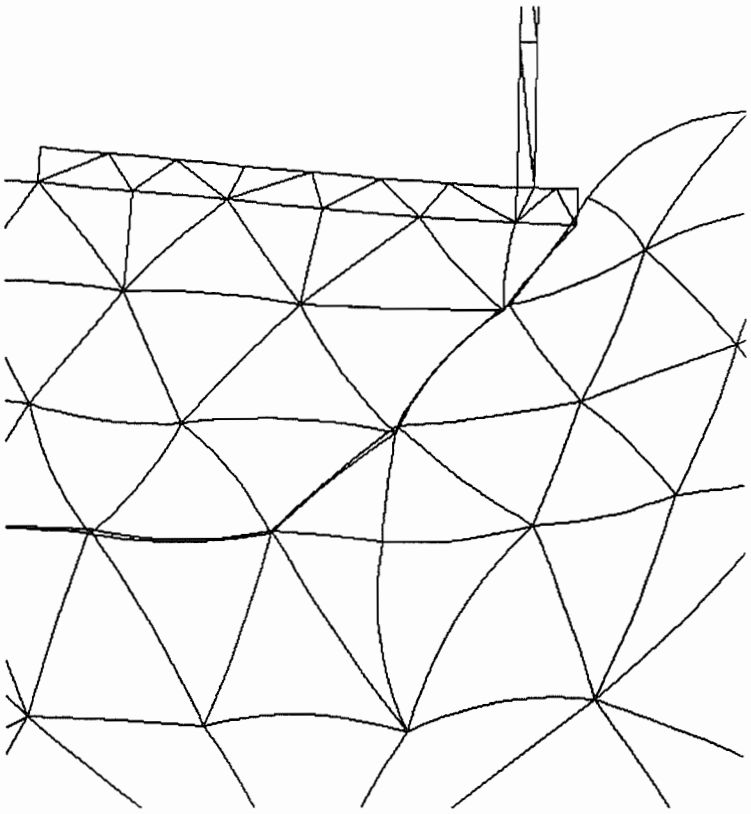

Figure 11.9: Deformed Mesh for run IV1 (After Burd *et al.* (1993))

The performance of the membrane in the analysis is assessed by studying the interface element Gauss point stresses at the end of run II5. The plot of the variation of normal stress along the membrane length (Figure 11.10) shows that σ is constant under the tank at about 200 *kPa*, due to the oil loading, and equal to the fill self weight outside of the annular plate. Directly under the tank wall σ reaches a peak of approximately 350 *kPa*, due to the extra imposed tank loading, and at the inside edge of the annular plate there is a stress relief, reducing σ to only 150 *kPa*, caused by the outwards rotation of the annular plate.

Figure 11.11 shows the mobilised angle of friction on the membrane (ϕ_i'), which is calculated from equation (11.7):-

$$\phi_i' = \tan^{-1}\left(\frac{\tau}{\sigma}\right) \tag{11.7}$$

where τ is the shear stress at the interface, (inwards acting shear is assumed positive, for Figure 11.11). For a distance of about 2 *m* beyond the outside edge of the annular plate the full friction angle of 10° is mobilised. This is followed by a sudden drop and sign change in the mobilised angle, caused by the reversal in direction of the shear stresses from outward to inward acting. This signifies that the soil below the membrane is being squeezed outwards from under the upper layer. Directly beneath the annular plate there is some mobilisation of friction, but insufficient to cause slipping. This is reflected in Figure 11.12, which shows the relative movement of the soil above the membrane compared to that below (u_r). The largest relative slipping, reaching a maximum of about 12 *mm*, is within 1 *m* of the tank wall centre-line, although the full friction is mobilised for a distance of up to 2 *m*. This is because beyond 1 *m* the normal stress is already very small and the nominal relative slip that occurs (i.e. < 1 *mm*) is enough to mobilise the full friction. The small relative movements under the annular plate are due to the finite shear stiffness of the interface elements (k_s) and are approximately equal to τ / k_s.

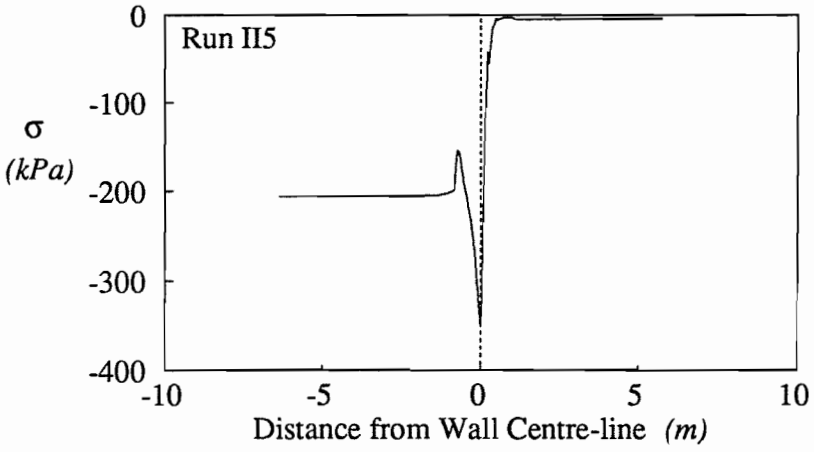

Figure 11.10: Normal Stress (σ) on Membrane

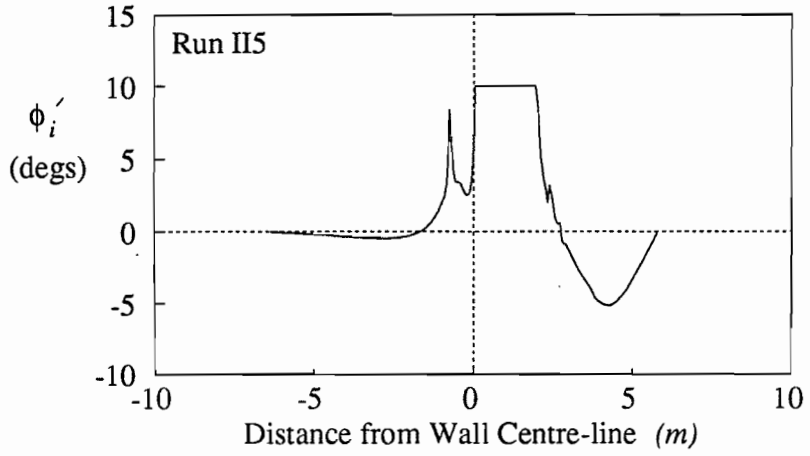

Figure 11.11: Mobilised Friction Angle (ϕ_i') on Membrane

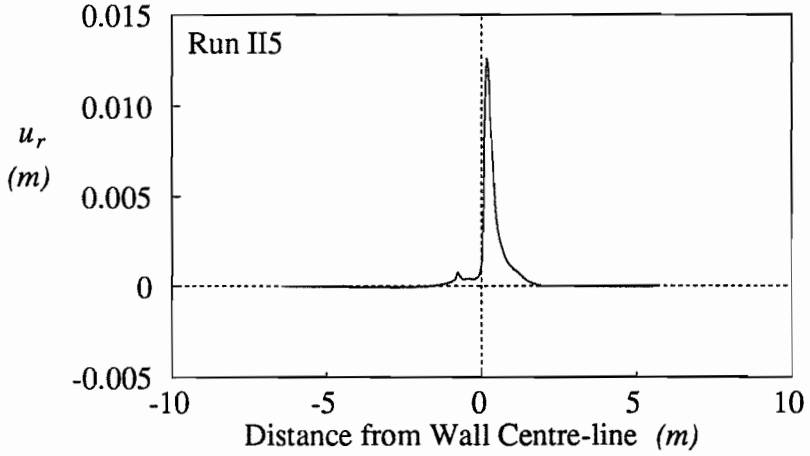

Figure 11.12: Relative Slip (u_r) along Membrane

11.6 Conclusions

This study demonstrates that the newly developed axisymmetric interface element formulation performs properly. It also provides a useful insight into the way low friction membranes influence the behaviour of granular bases for large oil storage tanks.

A sloping ended membrane is found to induce larger relative displacements ($\approx$ 37% maximum increase, for case considered) at the annular plate edge, than occur for a horizontally placed continuous membrane ($\approx$ 13% maximum increase), in comparison to the displacements which occur when no membrane is used.

The important conclusion to be drawn from this study is that the influence of the membrane is relatively small compared to the influence of the soil friction angle. By incorporating a membrane of friction angle 10°, the relative additional displacements incurred are equivalent to decreasing the peak fill friction angle by about 3° to 5°.

It is suggested that the returns obtained, in terms of safety and environmental protection, from incorporating a low friction impermeable membrane as a secondary containment within the base of a newly constructed oil tank, far outweigh the additional material costs involved.

CHAPTER 12:

CONCLUDING REMARKS

The large displacement, large strain, finite element code OXFEM was modified, as part of the research described in this thesis, to include both plane strain and axisymmetric elastic-perfectly frictional interface elements, as well as axisymmetric linear elastic membrane elements. These new formulations are capable of modelling large global displacements and finite rotations, although relative displacements within the interface element are constrained to being infinitesimal. The finite element equations are based on an Updated Lagrangian description of deformation.

The advantages of using interface elements are that, firstly they allow the properties of the soil-reinforcement interface to be varied independently of the soil properties and secondly they provide a convenient way of extracting the stresses acting at the soil-reinforcement boundary. Although the interface element material stiffness has been limited, in the calculations described in this thesis, to using only the purely elastic case for the sake of numerical stability, the stress updating procedure takes full account of plasticity ensuring that the overall solution for the stresses is correct.

The axisymmetric membrane formulation is rigorously verified through a series of closed form elastic test problems, with the elements placed at various inclinations. Similarly, the axisymmetric interface formulation is tested, but the difficulty of finding appropriate closed form test analyses has meant that the validation is less comprehensive for this element. For the tests undertaken, the finite element results show that the new formulations are reliable.

The new axisymmetric formulations are used in a limited number of parametric studies, along with a more comprehensive number of plane strain parametric studies, to investigate the effect of important variables within a two-layer soil system. It was initially envisaged that an analytical model, capable of predicting the behaviour of a two-layer soil system, would be developed from the parametric study results. However, this proved to be difficult because of the complex nature of the mechanisms acting in the system and was abandoned in favour of a detailed numerical analysis of the system. In fact it is now thought that no simple analytical design method can fully describe the behaviour of a two-layer soil system.

Two fundamental difficulties with developing a simple analytical method are modelling the exact load distribution through the fill and predicting the precise deformed shape of the membrane. It is shown that the normal stresses at the fill base are not only influenced by the presence of reinforcement, but also by the shear strength of the underlying clay. For an increase in the clay shear strength the load spread angle (for which there is no unique definition) reduces considerably. Therefore, the load distribution characteristics through the fill layer are not even specific to the fill material properties and the use of a load spread parameter that is a function only of fill properties is erroneous. Previous design methods also make inappropriate assumptions concerning the fixity of the membrane in order to assess the deformed shape, but from the reported results herein such fixity is clearly spurious.

Much discussion has recently centred on the problem of making analytical predictions of the reinforcement mechanisms for small surface displacements. It has been shown that in a small strain, plane strain, analysis where geometric non-linear effects are explicitly excluded from the computation, the reinforcement causes only a nominal improvement in the load spread through the fill layer (hitherto often thought to be the most important mechanism), but, more importantly, it significantly reduces both the magnitude and the area of influence of the shear stresses acting on the clay surface. The reinforcement attenuates the large detrimental outward acting shear stresses that occur in the unreinforced case and increases the amount of beneficial inward acting shear beyond the vertically loaded area. It

is this shear stress mechanism of the reinforcement that is responsible for the majority of the loading improvement in the small strain analyses and, in fact, the large strain (plane strain and axisymmetric) analyses too.

Although the Houlsby *et al.* (1989) and Houlsby and Jewell (1990) limit equilibrium methods are rational procedures for estimating the structural improvement for small displacements, through the shear stress mechanism, they idealize the arrangement of stresses and consider the fill material beneath the footing to be in a state of active failure. It has been shown, however, that even at large footing displacements this is not necessarily the case, for both plane strain and axisymmetry. Moreover, there is undoubtedly an additional stiffness and strength within the two-layer system once large displacements develop and the geometric non-linear effects of the tensioned membrane and restraint mechanisms, identified as operating in the large strain analyses, are introduced. This highlights the need for any design method to consider the different reinforcement effects which exist at small and large displacements.

Despite the limitations of the Houlsby *et al.* (1989) and Houlsby and Jewell (1990) methods, the comparative analytical predictions of the ultimate footing load (P_f) are found to be reasonable approximations to the finite element results (at a footing displacement of $0.6\,B;R$) for all of the small strain computations and, significantly, the plane strain and axisymmetric large strain reinforced computations. However, the predictions of P_f for the unreinforced large strain analyses and the values of the reinforcement force are less accurate, because of the afore-mentioned stress idealizations.

To obtain accurate analytical estimates of the reinforced P_f, appropriate values of the load spread angle (β) must be selected. It is suggested that Table 12.1 may be used for the general case of a "normal" strength fill layer ($\phi_{PS} \approx 40°$) of depth $D_f \leq B;R$ overlying clay of strength s_u, although these angles are approximations only ($\pm 5°$). Since the parametric study does not cover all the possible combinations of s_u, ϕ and D_f, a definitive estimate of β cannot be made. However, the relationship between these properties and β is derived qualitatively from the Meyerhof (1974) theory, given in equation (7.6).

s_u	β_{PS}	β_{Axi}
"Very soft" ($\approx 10\ kPa$)	60°	40°
"Soft" ($\approx 30\ kPa$)	40°	30°
"Firm" ($\approx 70\ kPa$)	30°	20°

Table 12.1: Approximate Plane Strain and Axisymmetric Load Spread Angles

A number of general conclusions relating to the behaviour of unreinforced and reinforced two-layer soil systems, deforming in plane strain and axisymmetry under the action of a single monotonic load, can be derived from the results of the large strain parametric study. It is clear that the presence of reinforcement has no appreciable influence on the load-displacement performance of the two-layer soil system within the elastic regime (i.e. for small surface displacements), compared to an unreinforced system. However, the reinforcement is shown to enhance the load bearing capacity of the system significantly, once plastic deformations occur, as observed frequently in practice and in the laboratory (e.g. Love (1984)).

The presence of reinforcement is found to have more effect for a thinner fill layer, than for a thicker layer. This conflicts with the implications of the Houlsby *et al.* (1989) and Houlsby and Jewell (1990) methods, which estimate greater lateral fill stresses for increases in fill thickness that consequently lead to a reduced unreinforced bearing capacity factor, and therefore the difference between the unreinforced and reinforced ultimate loads is larger for increasing fill thickness.

Using greater reinforcement stiffnesses results in improvements to the load-displacement response of the reinforced two-layer soil system, due to the increased contribution of the tensioned membrane mechanism. However, the benefit of increasing the reinforcement stiffness follows a pattern of diminishing returns, since larger shear stresses at the soil-reinforcement interface are generated, which induce higher reinforcement tensions, and consequently an arching effect develops in the fill. These additional shear stresses do not, in themselves, contribute to any structural improvement in the system. For

the cases studied a stiffness of the order 10^2 *kN/m* is perhaps the optimum range and there appears to be little further benefit beyond a modulus of around 3 000 *kN/m*. In fact the majority of the proprietary geosynthetics available, possess a stiffness within this suggested optimum range.

An important finding from the parametric study is that the length of the reinforcement needs to be sufficient to cover only the area of subgrade influenced by the normal and shear stresses acting at the interface. For a membrane of length just greater than this area of imposed load (i.e. $L \approx B + D_f \tan\beta$), the shear stress mechanism and the tensioned membrane effect can both operate adequately and provide a completely reinforced system. This contradicts any requirements for the membrane to be firmly anchored outside of the load spread area in order to attain a completely reinforced system.

A slightly different approach to that used for the main parametric study is employed to assess the influence of the membrane-soil friction angle. A low friction angle geosynthetic ($\phi_i = 10°$) is analysed, for a variety of different configurations, within a granular foundation. The results show that the displacements and soil deformations are not greatly increased, as might be expected, by introducing this potential plane of weakness. This illustrates the usefulness of placing impermeable low friction geosynthetics within foundations for fluid containment purposes.

The finite element formulations developed in this thesis are appropriate for the particular geotechnical problems considered. However, obvious improvements in the interface element formulation would be to incorporate a cohesive strength term and to allow large relative slip and even separation of the mating surfaces. These features should be included in any future work.

REFERENCES

Alenowicz, J. and Dembicki, E. (1990)
"Model tests on temporary road behaviour",
Proc. British Geotechnical Soc., Int. Reinforced Soil Conf., University of Strathclyde, Glasgow, UK

American Petroleum Institute Standard 650; Appendix I
"Welded steel tanks for oil storage - Undertank leak detection and subgrade protection",
American Petroleum Institute, Washington D.C., USA

Bathe K-J. (1982)
"Finite element procedures in engineering analysis",
Prentice-Hall, Inc., New Jersey, USA

Bell, R.W. (1991)
"The analysis of offshore foundations subjected to combined loading",
M.Sc. Thesis, University of Oxford, UK

Benham, P.P. and Crawford, R.J. (1987)
"Mechanics of engineering materials",
Longman Scientific and Technical, Harlow, UK

Bolton, M.D. (1979)
"A guide to soil mechanics",
The Macmillan Press Ltd., London, UK: pp 320-324

Bolton, M.D. (1986)
"The strength and dilatancy of sands",
Geotechnique, Vol. 36, No. 1: pp 65-78

Bourdeau, P.L. (1989)
"Modeling of membrane action in a two-layer reinforced soil system",
Computers and Geotechnics, Vol. 7, Nos. 1 and 2: pp 19-36

Brinch Hansen, J. (1970)
"A revised and extended formula for bearing capacity",
Bulletin No. 28, Danish Geotechnical Institute, Copenhagen, Denmark: pp 5-11

British Standard 2004 (1972)
"Code of practice for foundations",
British Standards Institution, London, UK: pp 20-21

Britto, A.M. and Gunn, M.J. (1987)
"Critical state soil mechanics via finite elements",
Ellis Horwood Ltd., Chichester, West Sussex, UK

Brown, J.D. and Paterson, W.G. (1964)
"Failure of an oil storage tank founded on a sensitive marine clay",
Canadian Geotechnical Journal, Vol. 1, No. 4:pp 205-214

Burd, H.J. (1986)
"A large displacement finite element analysis of a reinforced unpaved road",
D.Phil. Thesis, University of Oxford, UK

Burd, H.J. and Houlsby, G.T. (1986)
"A large strain finite element formulation for one dimensional membrane elements",
Computers and Geotechnics, Vol. 2, No. 1: pp 3-22

Burd, H.J. and Houlsby, G.T. (1989)
"Numerical modelling of reinforced unpaved roads",
Proc. 3rd Int. Symposium on Numerical Models in Geomechanics, Niagara, Canada: pp 699-706

Burd, H.J. and Houlsby, G.T. (1990)
"Finite element analysis of two cylindrical expansion problems involving nearly incompressible material behaviour",
Int. Journal for Numerical and Analytical Methods in Geomechanics, Vol. 14: pp 351-366

Burd, H.J. and Brocklehurst, C.J. (1990)
"Finite element studies of the mechanics of reinforced unpaved roads",
Proc. 4th Int. Conf. on Geotextiles, Geomembranes and Related Products, The Hague, Netherlands: pp 217-221

Burd, H.J. and Brocklehurst, C.J. (1991)
"Parametric studies of a soil reinforcement problem using finite element analysis",
Proc. 7th Int. Conf. of the Int. Association for Computer Methods and Advances in Geomechanics, Cairns, Queensland, Australia, Vol. 3: pp 1783-1788

Burd, H.J., Houlsby, G.T. and Brocklehurst, C.J. (1993)
"Analysis of the use of membranes in tank bases",
Confidential Report for British Petroleum, Engineering Science Department, University of Oxford, UK

Calladine, C.R. (1985)
"Plasticity for engineers",
Ellis Horwood Ltd., Chichester, West Sussex, UK

Craig, W.H. and Chua, K. (1990)
"Deep penetration of spud-can foundations on sand and clay",
Geotechnique, Vol. 40, No. 4: pp 541-556

Davies, M.C.R. and Bridle, R.J. (1990)
"Predicting the permanent deformation of reinforced flexible pavements subject to repeated loading",
Proc. British Geotechnical Soc., Int. Reinforced Soil Conf., University of Strathclyde, Glasgow, UK

Dawson, A.R. and Little, P.H. (1990)
"Reinforced haul-roads: Trials at Bothkennar, Scotland",
Proc. 4th Int. Conf. on Geotextiles, Geomembranes and Related Products, The Hague, Netherlands: p 250

Dawson, A.R. and Brown, S.F. (1992)
"Calibration and validation of design methods for geosynthetic haul roads",
Report No. PR92033, Dept. of Civil Engineering, University of Nottingham, UK

De Groot, M., Janse, E., Maagdenberg, T.A.C. and Van Den Berg, C. (1986)
"Design method and guidelines for geotextile application in road construction",
Proc. 3rd Int. Conf. on Geotextiles, Vienna, Austria: pp 741-746

Delmas, P., Matichard, Y., Gourc, J.P. and Riondy, G. (1986)
"Unsurfaced roads reinforced by geotextiles - a seven years experiment",
Proc. 3rd Int. Conf. on Geotextiles, Vienna, Austria: pp 1015-1020

Dembicki, E. and Jermolowicz, P. (1991)
"Soil-geotextile interaction",
Geotextiles and Geomembranes, Vol. 10, No. 3: pp 249-268

Drucker, D.C. and Prager, W.J. (1952)
"Soil mechanics and plastic analysis or limit design",
Quarterly Journal of Applied Mathematics, Vol. 10, No. 2: pp 157-165

Fannin, R.J. (1986)
"Geogrid reinforcement of granular layers on soft clay",
D.Phil. Thesis, University of Oxford, UK

Frank, R., Guenot, A. and Humbert, P. (1982)
"Numerical analysis of contacts in geomechanics",
Proc. 4th Int. Conf. on Numerical Methods in Geomechanics, Edmonton, Canada, Vol. 1: pp 37-45

Gens, A., Carol, I. and Alonso, E.E. (1989)
"An interface element formulation for the analysis of soil-reinforcement interaction",
Computers and Geotechnics, Vol 7, No 1-2: pp 133-151

Giroud, J.P. and Noiray, L. (1981)
"Geotextile-reinforced unpaved road design",
Proc. ASCE, Journal of the Geotechnical Engineering Division, 107 (GT9): pp 1233-1254

Giroud, J.P., Ah-Line, C. and Bonaparte, R. (1984)
"Design of unpaved roads and trafficked areas with geogrids",
Proc. Symposium on Polymer Grid Reinforcement in Civil Engineering, Thomas Telford Ltd., London, UK: pp 116-127

Giroud, J.P. (1986)
"From geotextiles to geosynthetics: a revolution in geotechnical engineering"
Proc. 3rd Int. Conf. on Geotextiles, Vienna, Austria: pp 1-18

Goodman, R.E., Taylor, R.L. and Brekke, T.L. (1968)
"A model for the mechanics of jointed rock",
Proc. ASCE, Journal of the Soil Mechanics and Foundations Division, 94 (SM3): pp 637-659

Griffiths, D.V. (1982)
"Computation of bearing capacity on layered soils",
Proc. 4th Int. Conf. on Numerical Methods in Geomechanics, Edmonton, Canada: pp 163-170

Griffiths, D.V. (1985)
"Numerical modelling of interfaces using conventional finite elements",
Proc. 5th Int. Conf. on Numerical Methods in Geomechanics, Nagoya, Japan: pp 837-844

Hammit, G.M. (1970)
"Thickness requirements for unsurfaced roads and airfields, bare base support",
Project 3782-65, TR2-70-5, Soils and Pavements Laboratory, U.S. Army Engineer Waterways Experiment Station, Vicksburg, Mississippi, USA

Handel, E., Schweiger, H.F. and Yeo, K.C. (1990)
"A simple thin-layer element to model soil-geotextile interaction",
Proc. British Geotechnical Soc., Int. Reinforced Soil Conf., University of Strathclyde, Glasgow, UK

Hanna, A.M. and Meyerhof, G.G. (1980)
"Design charts for ultimate bearing capacity of foundations on sand overlaying soft clay",
Canadian Geotechnical Journal, Vol. 17, No. 2: pp 300-303

Hird, C.C. and Kwok, C.M. (1989)
"Finite element studies of interface behaviour in reinforced embankments on soft ground",
Computers and Geotechnics, Vol. 8, No. 2: pp 111-131

Hird, C.C. and Kwok, C.M. (1990)
"Parametric studies of the behaviour of a reinforced embankment",
Proc. 4th Int. Conf. on Geotextiles, Geomembranes and Related Products, The Hague, Netherlands: pp 137-142

Hird, C.C. and Pyrah, I.C. (1990)
"Class A predictions of the behaviour of a reinforced embankment on soft ground",
Proc. British Geotechnical Soc., Int. Reinforced Soil Conf., University of Strathclyde, Glasgow, UK

Houlsby, G.T. (1988)
"Finite element mesh generation program OXMESH",
Unpublished Report, Engineering Science Department, University of Oxford, UK

Houlsby, G.T., Milligan, G.W.E., Jewell, R.A. and Burd, H.J. (1989)
"A new approach to the design of unpaved roads - Part I",
Ground Engineering, Vol. 22, No. 3: pp 25-29

Houlsby, G.T. and Jewell, R.A. (1990)
"Design of reinforced unpaved roads for small rut depths",
Proc. 4th Int. Conf. on Geotextiles, Geomembranes and Related Products, The Hague, Netherlands: pp 171-176

Houlsby, G.T. (1991)
"How the dilatancy of soils affects their behaviour",
Report No. OUEL 1888/91, Engineering Science Department, University of Oxford, UK

Houlsby, G.T. (1992)
Personal communication

Jaumann, G. (1911)
Sitzungsberichte Akad. Wiss. Wien (IIa) 120: p 385

Jewell, R.A. and Wroth, C.P. (1987)
"Direct shear tests on reinforced sand",
Geotechnique, Vol. 37, No. 1: pp 53-68

Jewell, R.A. (1991)
Personal communication

John, N.W.M. (1987)
"Geotextiles",
Blackie and Son Ltd., London, UK

Kodikara, J.K. and Moore, I.D. (1991)
"A versatile interaction analysis for nonlinear bodies",
Proc. 7th Int. Conf. of the Int. Association for Computer Methods and Advances in Geomechanics, Cairns, Queensland, Australia, Vol. 2: pp 1171-1176

Koerner, R.M. (1986)
"Designing with geosynthetics",
Prentice-Hall International Ltd., London, UK

Kwok, C.M. (1987)
"Finite element studies of reinforced embankments on soft ground",
Ph.D. Thesis, University of Sheffield, UK

Little, P.H. (1992)
"Calibration and validation of design methods for geosynthetic reinforced haul roads",
Ph.D Thesis, University of Nottingham, UK

Love, J.P. (1984)
"Model testing of geogrids in unpaved roads",
D.Phil. Thesis, University of Oxford, UK

Love, J.P., Burd, H.J., Milligan, G.W.E. and Houlsby, G.T. (1987)
"Analytical and model studies of reinforcement of a layer of granular fill on a soft clay subgrade",
Canadian Geotechnical Journal, Vol. 24, No. 4: pp 611-622

Matsuoka, H. (1976)
"On the significance of the spatial mobilised plane",
Soils and Foundations, Vol. 16(1): pp 91-100

Meyerhof, G.G. (1974)
"Ultimate bearing capacity of footings on sand layer overlaying clay",
Canadian Geotechnical Journal, Vol. 11, No. 2: pp 223-229

Milligan, G.W.E. and Love, J.P. (1984)
"Model testing of geogrids under an aggregate layer on soft ground",
Proc. Symposium on Polymer Grid Reinforcement in Civil Engineering, Thomas Telford Ltd., London, UK: pp 128-138

Milligan, G.W.E., Fannin, J. and Farrar, D.M. (1986)
"Model and full-scale tests of granular layers reinforced with a geogrid",
Proc. 3rd Int. Conf. on Geotextiles, Vienna, Austria: pp 61-66

Milligan, G.W.E., Jewell, R.A., Houlsby, G.T. and Burd, H.J. (1989)
"A new approach to the design of unpaved roads - Part II",
Ground Engineering, Vol. 22, No. 8: pp 37-42

Moore, I.D. and Booker, J.R. (1989)
"Geometrically nonlinear analysis of buried cylinders",
Proc. 3rd Int. Symposium on Numerical Models in Geomechanics, Niagara, Canada: pp 716-723

Nagtegaal, J.C., Parks, D.M. and Rice, J.R. (1974)
"On numerically accurate finite element solutions in the fully plastic range",
Computer Methods in Applied Mechanics and Engineering, Vol. 4: pp 153-177

Nieuwenhuis, J.D. (1977)
"Membranes and the bearing capacity of roadbases",
Proc. Int. Conf. on Geotextiles, Paris, France: pp 3-8

Nixon, I.K. (1949)
"$\phi = 0$ Analysis",
Geotechnique, Vol. 1, No. 3: pp 208-209

Perloff, W.H. and Baron, W. (1976)
"Soil mechanics, principles and applications",
John Wiley and Sons Inc., New York, USA: pp 186-188

Pike, D.C., Ascott, S.M. and Leech, R.M. (1977)
"Sub-base stability: a shear-box test compared with other prediction methods",
Transport and Road Research Laboratory, Laboratory Report 785, Berkshire, UK

Poran, C.J. (1985)
"Bearing capacity of geogrid-reinforced granular-base overlaying soft clay",
Ph.D. Thesis, University of California, Davis, USA

Roscoe, K.H. and Burland, J.B. (1968)
"On the generalised stress-strain behaviour of 'wet' clay",
In "Engineering plasticity", Ed. by J. Heyman and F. A. Leckie, Cambridge University Press, UK: pp 535-609

Sagaseta, C. (1984)
"Quasi-static undrained expansion of a cylindrical cavity in clay in the presence of shaft friction and anisotropic initial stresses",
Unpublished Research Report, Engineering Science Department, University of Oxford, UK

Sellmeijer, J.B., Kenter, C.J. and Van Den Berg, C. (1982)
"Calculation method for a fabric reinforced road",
Proc. 2nd Int. Conf. on Geotextiles, Las Vegas, USA: pp 393-398

Sellmeijer, J.B. (1990)
"Design of geotextile reinforced paved roads and parking areas",
Proc. 4th Int. Conf. on Geotextiles, Geomembranes and Related Products, The Hague, Netherlands: pp 177-182

Slater, R.A.C. (1977)
"Engineering plasticity - Theory and application to metal forming processes",
The Macmillan Press Ltd., London, UK: pp 263-266

Sloan, S.W. (1981)
"Numerical analysis of incompressible and plastic solids using finite elements",
Ph.D. Thesis, University of Cambridge, UK

Sowers, G.F., Collins, S.A. and Millar, D.G. (1982)
"Mechanism of geotextile-aggregate support in low-cost roads",
Proc. 2nd Int. Conf. on Geotextiles, Las Vegas, USA: pp 341-346

Specification for Highway Works (1986)
"Notes for guidance on, and the specification for highway works - Part 3, Series 800",
Department of Transport, H.M.S.O., London, UK

Taylor, D.W. (1965)
"Fundamentals of soil mechanics",
John Wiley and Sons Inc., New York, USA: pp 609-611

Teh, C-I. (1987)
"An analytical study of the cone penetration test",
D.Phil. Thesis, University of Oxford, UK

Terzaghi, K. (1944)
"Theoretical soil mechanics",
John Wiley and Sons Inc., New York, USA

Timoshenko, S. and Goodier, J.N. (1951)
"Theory of elasticity",
Second edition, McGraw-Hill, London, UK

Vesic, A.S. (1975)
"Bearing capacity of shallow foundations",
"Foundation Engineering Handbook", Ed. by H. F. Winterkorn and H. Y. Fang, Van Nostrand Reinhold, New York, USA: pp 121-147

Wroth, C.P. (1984)
"The interpretation of in situ soil tests",
Twenty-fourth Rankine Lecture, Geotechnique, Vol. 34, No. 4: pp 449-489

Wroth, C.P. and Houlsby, G.T. (1985)
"Soil mechanics - property characterization and analysis procedures",
Proc. 11th Int. Conf. on Soil Mechanics and Foundation Engineering, San Francisco, USA, Vol. 1:pp 1-57

Yu, H-S. (1990)
"Cavity expansion theory and its application to the analysis of pressuremeters",
D.Phil. Thesis, University of Oxford, UK

Zaman, M.M. (1985)
"Evaluation of 'thin-layer element' and modelling of interface behaviour in soil-structure interaction",
Proc. 5th Int. Conf. on Numerical Methods in Geomechanics, Nagoya, Japan: pp 1797-1803

Zeevaert, A.E. (1980)
"Finite element formulation for the analysis of interfaces, nonlinear and large displacement problems in geotechnical engineering",
Ph.D. Thesis, Georgia Institute of Technology, Atlanta, Georgia, USA

Zienkiewicz, O.C., Best, B., Dullage, C. and Stagg, K.G. (1970)
"Analysis of non-linear problems in rock mechanics with particular reference to jointed rock systems",
Proc. 2nd Int. Cong. on Rock Mechanics, Belgrade, Vol. 2: pp 501-509

Zienkiewicz, O.C. (1977)
"The finite element method",
Third edition, McGraw-Hill, London, UK